The Plant Cell, Vol. 25: 2714–2730, July 2013, www.plantcell.org

Constitutively Elevated Salicylic Acid Levels Alter Photosynthesis and Oxidative State but Not Growth in Transgenic *Populus*[C][W]

Liang-Jiao Xue,[a,b,c] Wenbing Guo,[a,b,1] Yinan Yuan,[d] Edward O. Anino,[a,b,2] Batbayar Nyamdari,[a,b] Mark C. Wilson,[c] Christopher J. Frost,[a,b,3] Han-Yi Chen,[a] Benjamin A. Babst,[a,b,4] Scott A. Harding,[a,b] and Chung-Jui Tsai[a,b,c,5]

[a] Warnell School of Forestry and Natural Resources, University of Georgia, Athens, Georgia 30602
[b] Department of Genetics, University of Georgia, Athens, Georgia 30602
[c] Institute of Bioinformatics, University of Georgia, Athens, Georgia 30602
[d] School of Forest Resources and Environmental Science, Michigan Technological University, Houghton, Michigan 49931

ORCID IDs: 0000-0003-1766-5298 (L-J.X.); 0000-0003-1688-7286 (M.C.W.); 0000-0001-5657-0633 (B.A.B.); 0000-0002-9282-7704 (C-J.T.).

Salicylic acid (SA) has long been implicated in plant responses to oxidative stress. SA overproduction in *Arabidopsis thaliana* leads to dwarfism, making in planta assessment of SA effects difficult in this model system. We report that transgenic *Populus tremula* × *alba* expressing a bacterial SA synthase hyperaccumulated SA and SA conjugates without negative growth consequences. In the absence of stress, endogenously elevated SA elicited widespread metabolic and transcriptional changes that resembled those of wild-type plants exposed to oxidative stress-promoting heat treatments. Potential signaling and oxidative stress markers azelaic and gluconic acids as well as antioxidant chlorogenic acids were strongly coregulated with SA, while soluble sugars and other phenylpropanoids were inversely correlated. Photosynthetic responses to heat were attenuated in SA-overproducing plants. Network analysis identified potential drivers of SA-mediated transcriptome rewiring, including receptor-like kinases and *WRKY* transcription factors. Orthologs of *Arabidopsis* SA signaling components *NON-EXPRESSOR OF PATHOGENESIS-RELATED GENES1* and thioredoxins were not represented. However, all members of the expanded *Populus* nucleoredoxin-1 family exhibited increased expression and increased network connectivity in SA-overproducing *Populus*, suggesting a previously undescribed role in SA-mediated redox regulation. The SA response in *Populus* involved a reprogramming of carbon uptake and partitioning during stress that is compatible with constitutive chemical defense and sustained growth, contrasting with the SA response in *Arabidopsis*, which is transient and compromises growth if sustained.

INTRODUCTION

Salicylic acid (SA) is a phytohormone regulating many aspects of plant growth and adaptation, including photosynthesis, transpiration, thermogenesis, oxidative stress response, and disease resistance (reviewed in Vlot et al., 2009; Rivas-San Vicente and Plasencia, 2011). SA biosynthesis and signaling have been most extensively studied in *Arabidopsis thaliana*, especially in relation to basal defense and systemic acquired resistance (SAR) (Dong, 2001; Loake and Grant, 2007). SA accumulation is also part of the abiotic stress (e.g., ozone, UV, or heat) response, associated with cellular redox change and defense gene stimulation (Yalpani et al., 1994; Sharma et al., 1996; Larkindale and Knight, 2002). Although SA is ubiquitous in plants, species-specific differences in SA level or effects have been reported (Raskin, 1992). In the woody perennial *Populus* spp, the role of SA in disease resistance has not been substantiated (Germain and Séguin, 2011), and both SA abundance and involvement in stress (e.g., ozone) tolerance and defense gene activation exhibit genotypic differences (Koch et al., 2000; Vahala et al., 2003; Diara et al., 2005).

SA biosynthesis and overall homeostasis differ in fundamental ways between *Arabidopsis* and *Populus*. Stress-induced SA synthesis in *Arabidopsis* occurs in the chloroplast and is mediated by ISOCHORISMATE SYNTHASE1 (Wildermuth et al., 2001; Garcion et al., 2008), a function that appears to have evolved following genome duplication in the *Arabidopsis* lineage (Yuan et al., 2009). By contrast, the single-copy ortholog of *Populus* retains the ancestral isochorismate synthase function in phylloquinone biosynthesis, while SA originates from cinnamic acid via the cytosolic phenylpropanoid pathway (Figure 1) (Yuan et al., 2009). Ambient levels of SA in *Populus* are substantially higher than those reported in *Arabidopsis* (Nawrath and Métraux, 1999; Koch et al., 2000; Wildermuth et al., 2001), where constitutively elevated SA has been associated with dwarfism (reviewed in Rivas-San Vicente

[1] Current address: Guangdong Academy of Forestry, Guangzhou, 510520 China.
[2] Current address: University of Eldoret, Eldoret, 30100, Kenya.
[3] Current address: Medical Imaging Consultants, Gainesville, FL 32606.
[4] Current address: Biosciences Department, Brookhaven National Laboratory, Upton, NY 11973.
[5] Address correspondence to cjtsai@uga.edu.
The author responsible for distribution of materials integral to the findings presented in this article in accordance with the policy described in the Instructions for Authors (www.plantcell.org) is: Chung-Jui Tsai (cjtsai@uga.edu).
[C] Some figures in this article are displayed in color online but in black and white in the print edition.
[W] Online version contains Web-only data.
www.plantcell.org/cgi/doi/10.1105/tpc.113.112839

and Plasencia, 2011). In several *Arabidopsis* SA mutants, the observed growth retardation has been attributed to impaired photosynthesis (Mateo et al., 2006). Higher levels of SA, either exogenously applied or genetically varied, induce stomatal closure and decrease photosynthetic activity in many species, probably via reactive oxygen species (ROS) signaling (Lee, 1998; Mori et al., 2001; Mateo et al., 2006). Stomatal closure appears to be a common response to a number of abiotic (UV, ozone, and salt) (Nogués et al., 1999; Vahala et al., 2003; Poór et al., 2011) or biotic stresses (Lee et al., 1999; Melotto et al., 2006) that stimulate SA accumulation (Gaffney et al., 1993; Yalpani et al., 1994). The emerging view of stomata as an integral component of biotic and abiotic stress responses supports a complex crosstalk between photosynthesis, redox, and defense that involves SA signaling (Zeng et al., 2010).

SA may also interface directly with *Populus* chemical defense due to its structural similarity to salicin (salicyl alcohol glucoside; Figure 1), the core component of phenolic glycosides (PGs; salicinoids). Despite their quantitative and adaptive significance as defense chemicals in Salicaceae (*Populus* and *Salix*), the biosynthetic pathway of PGs remains poorly understood (Tsai et al., 2006; Boeckler et al., 2011). SA is known to be a decomposition product of PGs, dating back to their linked discoveries for medicinal uses of Salicaceae bark (reviewed in Pierpoint, 1994; Mahdi et al., 2006). However, the utilization of SA as a direct precursor for PG biosynthesis has not been supported by feeding or tracer experiments (Zenk, 1967; Payyavula et al., 2009; Babst et al., 2010) or by transgenic expression of bacterial SA hydroxylase (NahG) in *Populus* (Morse et al., 2007). Regardless, both SA and PGs share the same phenylpropanoid origin in *Populus* (Yuan et al., 2009; Babst et al., 2010), suggesting a potential metabolic link that may be sensitive to various defense and adaptive functions.

In this study, we engineered the bacterial SA biosynthesis and degradation pathways into *Populus tremula* × *alba* (clone 717-1B4) and generated metabolite and gene correlation networks for investigating SA function. Our findings suggest that SA increases of two to three orders of magnitude elicited strong oxidative stress responses in *Populus* without compromising growth. Network analysis identified metabolite and gene clusters associated with changing carbon inputs, phenylpropanoid homeostasis, and redox regulation during *Populus* responses to elevated SA. We discuss the findings in light of the pleiotropic functions of SA in modulating stomatal behavior, chemical defense, and oxidative stress responses in *Populus*.

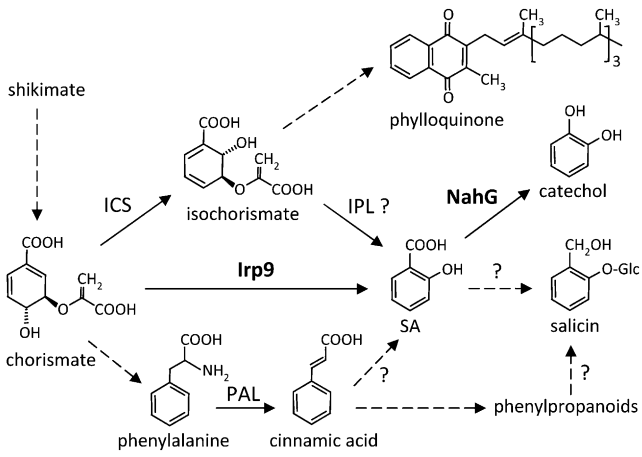

Figure 1. SA Biosynthetic Pathways from Isochorismate or Phe and Their Downstream Metabolites.

Reactions catalyzed by Irp9 and NahG are shown in boldface. Dashed arrows indicate multistep pathways, and question marks denote unresolved biosynthetic steps.

RESULTS

Characterization of Transgenic Poplar with Altered SA Levels

The bifunctional SA synthase gene *Irp9* from the pathogenic bacterium *Yersinia enterocolitica* (Pelludat et al., 2003) was introduced into *P. tremula* × *alba* (clone 717-1B4) under the control of a constitutive (cauliflower mosaic virus 35S) promoter, with or without the plastid-targeting sequence from the *Arabidopsis* ferredoxin (*FD*) gene. Hereafter, transgenic plants with plastidic or cytosolic targeting of the transgene are referred to as FD-Irp9 and Irp9, respectively. The third group of transgenic plants harbors the *Pseudomonas putida NahG* gene, also driven by the cauliflower mosaic virus 35S promoter (Gaffney et al., 1993). Eight to 11 putative transgenic lines were obtained for each group, and lines with high levels of transgene expression were identified by quantitative RT-PCR (qRT-PCR) (see Supplemental Figures 1A to 1C online). HPLC–time-of-flight mass spectrometry (TOF/MS) analysis identified a range of SA metabolic phenotypes from leaf methanolic extracts of transgenic plants (see Supplemental Figures 1D and 1E online). FD-Irp9 plants exhibited elevated levels of SA conjugates, including SA-glucoside (SAG), gentisic acid glucoside (GAG), and, to a much smaller extent, SA Glc ester. The levels of SA metabolites were highest in line F10, followed by F55 and F52, in accordance with the estimated *FD-Irp9* transcript abundance (see Supplemental Figures 1A to 1C online). Cytosolic Irp9 had a minor effect on SA conjugate levels. The three NahG lines examined (N31, N24, and N51) exhibited reduced levels of SA conjugates, consistent with previous findings (Morse et al., 2007).

Effects of SA Manipulation on Photosynthesis, Stomatal Behavior, Growth, and Membrane Integrity under Different Temperature Regimes

Wild-type and selected transgenic plants were vegetatively propagated to assess the effects of SA perturbation on photosynthesis, growth, metabolite, and gene expression responses. Two temperature regimes (27°/17°C normal temperature [NT] versus 35°/25°C high temperature [HT], day/night) were used because heat stress is known to accelerate photosynthesis and promote oxidative stress (Allakhverdiev et al., 2008; Weston et al., 2011) and because SA has been implicated in heat stress response (Larkindale and Knight, 2002; Clarke et al., 2004) and stomatal closure (Mateo et al., 2006). Photosynthesis was

monitored over a period of 19 d when growth temperatures were varied from NT to HT and then back to NT (see Methods), using the wild type and two lines each of the FD-Irp9 (F52 and F55) and NahG (N24 and N31) transgenics. Repeated measures analysis of variance (ANOVA) revealed significant differences in photosynthetic properties of both young (leaf plastochron index LPI-5) and mature (LPI-10) source leaves over time, reflecting significant treatment effects (Figure 2). Significant genotypic differences were also detected, and the responses were stronger in mature leaves than young leaves. Overall, net photosynthesis, stomatal conductance, and transpiration rates increased significantly at HT, similar to those reported for temperate *Populus* species (Hozain et al., 2010; Weston et al., 2011). However, the responses were significantly attenuated in the mature source leaves of FD-Irp9 plants. As a result, FD-Irp9 lines exhibited significantly reduced net photosynthesis, stomatal conductance, and transpiration relative to the wild type under HT growth (Figure 2; see Supplemental Table 1 online).

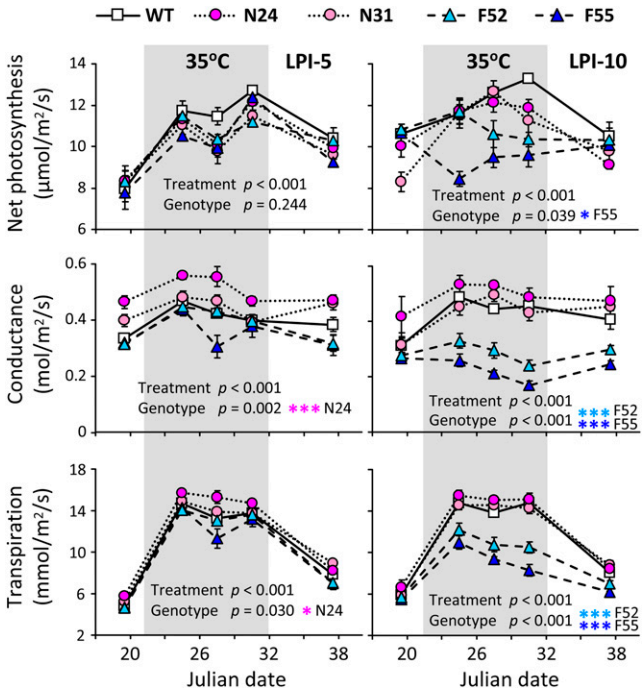

Figure 2. Leaf Photosynthetic Characteristics under Varying Growth Temperatures.

Net photosynthesis, stomatal conductance, and transpiration were measured in young (LPI-5) and mature (LPI-10) source leaves of the wild type (WT) and two independent lines each from the FD-Irp9 (F52 and F55) and NahG (N24 and N31) transgenics. Error bars are SD of three to 10 biological replicates. The effects of treatment or genotype were assessed by repeated measures ANOVA and indicated by P values. Significant genotypic effects were further analyzed by pairwise comparison between wild-type and individual transgenic lines, as denoted by asterisks (***$P \leq 0.01$, **$0.01 < P \leq 0.05$, and *$0.05 < P \leq 0.1$; see Supplemental Table 1 online).

[See online article for color version of this figure.]

A separate cohort of plants derived from the wild type and two to three lines each of the Irp9 (I6 and I8), FD-Irp9 (F10, F52, and F55), and NahG (N24, N31, and N51) transgenic lines was randomly assigned to two growth chambers and maintained under identical (NT) conditions. After 50 d, one chamber was changed to HT for 1 week before returning to NT for recovery. Plant height was monitored over the 2-month period. Although initial plant size varied, increment height growth did not differ significantly among genotypes under either temperature regime (Figures 3A and 3B). The results were confirmed using another cohort of plants under greenhouse conditions (Figures 3C and 3D). The data suggested that unlike in *Arabidopsis* (Rivas-San Vicente and Plasencia, 2011), growth was not compromised by constitutive overproduction of SA in *Populus*.

Leaf (LPI-6) tissues from wild-type and transgenic lines exhibited similar electrolyte leakage regardless of treatment (see Supplemental Figures 2A and 2B online), suggesting the absence of any transgenic or HT effect on plasma membrane integrity. The levels of total cellular electrolytes (released after boiling) were increased by HT treatments in wild-type, Irp9, and NahG lines, but not in the FD-Irp9 plants (see Supplemental Figures 2A and 2B online), suggesting altered cellular metabolism in response to HT. The lack of genotypic differences in electrolyte leakage was confirmed in a separate test using leaves from greenhouse-grown wild-type and F10 plants (see Supplemental Figure 2C online). Together, the data suggested that neither SA nor HT caused cellular membrane damage but that SA-overproducing plants exhibited lower total cellular electrolytes than the other plant lines during HT growth, indicative of distinct metabolic adjustments.

Altered Leaf Soluble Phenylpropanoid Composition Caused by SA Perturbation

Metabolite profiling of young source leaves (LPI-5) from heat-treated and unstressed plants (the wild type, I6, I8, F10, F52, F55, N24, N31, and N51) was performed using HPLC–TOF/MS and gas chromatography–mass spectrometry (GC-MS) to gauge the metabolic responses to SA manipulation and/or the temperature regime. The genotypic differences (relative to the wild type) observed from preliminary screening for SA-related metabolites were confirmed. Under NT, the SAG increases were most pronounced in F10 (~800-fold), followed by F55 and F52 (258- and 165-fold, respectively) (Figure 4; see Supplemental Data Set 1 online). GAG levels increased by ~17- to 34-fold, while free SA levels rose slightly (1.3- to 2.7-fold) in these lines. We found statistically significant but small (approximately twofold) increases of SAG and GAG in Irp9 plants as well, suggesting low levels of cytosolic chorismate-to-SA conversion. The SA degradation product catechol accumulated as catechol glucoside in NahG plants, at approximately fourfold higher levels than in the wild type (see Supplemental Data Set 1 online). Heat treatment induced a further increase of free SA and SAG, by up to fourfold, exclusively in the FD-Irp9 lines. An overall similar pattern was observed for LPI-1, a newly emerged sink leaf, although SA conjugates were detected at slightly lower levels than in LPI-5 (Figure 4). Because SA and SAG are interconvertible, both capable of inducing defense gene expression and an

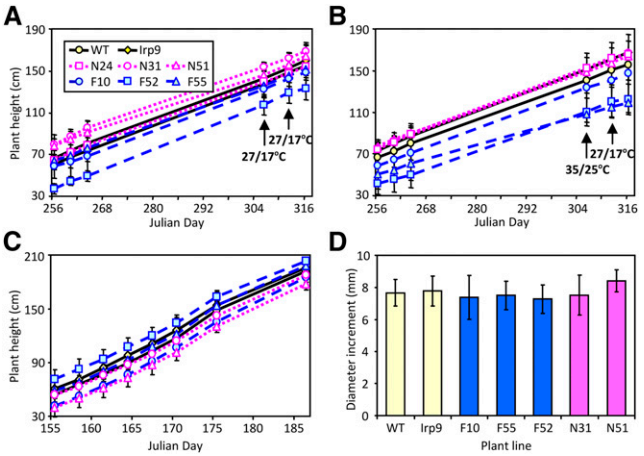

Figure 3. Growth of Wild-Type and Transgenic *Populus*.

(A) to **(B)** Height growth of plants maintained under ambient temperatures **(A)** or ambient temperatures interrupted by a 1-week exposure to elevated temperatures **(B)**. Data represent means ± SD, n = 8 to 9 for the wild type (WT), 7 to 9 for Irp9 (combined from two independent lines), 2 to 4 for FD-Irp9 (F) lines, and 3 to 5 for NahG (N) lines. Height increment per unit time did not differ significantly among genotypes based on repeated measures ANOVA (P = 0.52 and 0.73 for **[A]** and **[B]**, respectively).
(C) to **(D)** Height growth **(C)** and diameter increment **(D)** of plants maintained in a greenhouse over one summer month. n = 6 for the wild type, 3 for Irp9, 2 to 5 for F lines, and 3 to 4 for N lines. Height increment per unit time did not differ significantly based on repeated measures ANOVA (P = 0.37). No significant difference was found for diameter increment between wild-type and individual transgenic lines during the monitoring period based on the two-sample t test.
[See online article for color version of this figure.]

oxidative burst (Hennig et al., 1993; Kawano et al., 2004), and because both were significantly elevated in the FD-Irp9 lines, we refer to the FD-Irp9 plants (or transgenic effects) as SA-hyperaccumulating for simplicity of description.

Salicinoids are among the most abundant soluble phenolic metabolites in the experimental *Populus* clone 717-1B4. At NT, the two major PGs, salicortin and tremulacin, were reduced by ~20 to 40% in FD-Irp9 but were increased by ~20 to 30% in the NahG lines (see Supplemental Data Set 1 online). HT reduced foliar PG levels overall, but not in FD-Irp9 lines where PG levels were already low prior to HT treatment (see Supplemental Data Set 1 online). Regression analysis showed that total PG levels (salicin, salicortin, and tremulacin) correlated positively with total SA (SA and SA conjugates) in wild-type and Irp9 lines at both NT and HT, but they correlated negatively in the FD-Irp9 lines (see Supplemental Figure 3 online). The results did not support SA as being a direct precursor of PGs but were indicative of metabolic competition between SA and PG accrual. Levels of chlorogenic acids (including caffeoylquinic acid isomers 3-CQA, 4-CQA, and 5-CQA), another class of abundant soluble phenolics, were also reduced by heat. Unlike PGs, however, levels of chlorogenic acids correlated positively with SA metabolites in all genotypes, although the trend was weak in FD-Irp9 lines (see Supplemental Figure 3 online). Further analysis of individual isomers revealed two distinct patterns in response to HT or SA perturbation (see Supplemental Data Set 1 and Supplemental Figure 3 online). Whereas the predominant 5-CQA was sensitive to HT but insensitive to SA, the reverse was true for the two less abundant isomers 3-CQA and 4-CQA, pointing to a potential role of chlorogenic acid isomerization in response to elevated SA.

Altered Primary Metabolite Responses to HT in SA-Hyperaccumulating Plants

Tricarboxylic acid (TCA) cycle intermediates citrate, malate, 2-oxoglutarate, succinate, and fumarate did not differ between genotypes under NT. HT treatment increased the levels of TCA cycle intermediates, as previously reported in *Arabidopsis* (Kaplan et al., 2004), but only in wild-type, Irp9, and NahG poplar lines (see Supplemental Data Set 1 online). TCA metabolite levels remained largely unchanged in the FD-Irp9 lines at HT, reminiscent of the pattern observed for total cellular electrolytes (see Supplemental Figure 2 online). Inositol, xylitol, and, to a smaller extent, galactitol were elevated by HT regardless of genotype (see Supplemental Data Set 1 online). The increases of these metabolites therefore represent a general stress response. Suc levels did not change significantly among genotypes or due to temperature. The predominant hexoses (Glc and Fru) and pentose (Xyl) were reduced in the wild-type, Irp9, and NahG

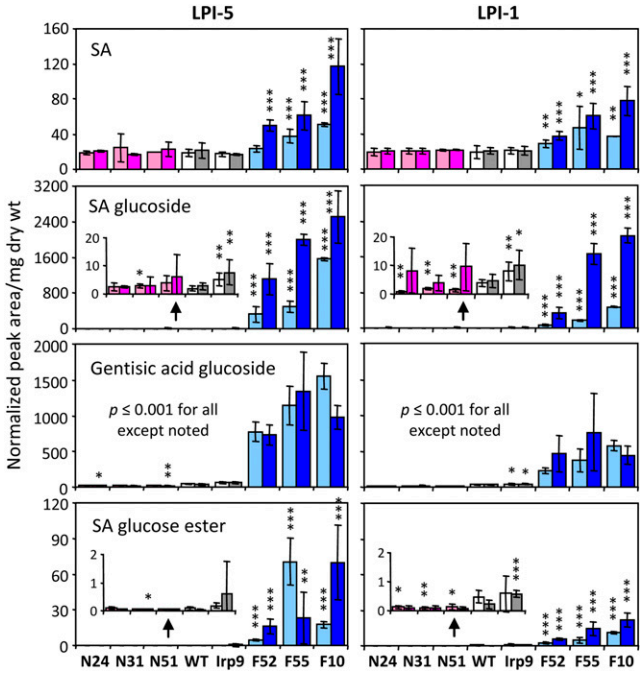

Figure 4. Relative Abundance of SA and SA-Related Conjugates.

Samples are color-coded by plant group. Lighter and darker bars denote normal and high temperatures, respectively. Values are means ± SD of n = 7 to 10 for wild-type (WT) and Irp9 plants, n = 2 to 3 for FD-Irp9 (F) lines, and n = 3 to 5 for NahG (N) lines. Statistical significance between wild-type and individual transgenic lines was evaluated by the two-sample t test (***P ≤ 0.001, **0.001< P ≤ 0.01, and *0.01< P ≤ 0.05). dry wt, dry weight.
[See online article for color version of this figure.]

plants during HT growth by ~70% (see Supplemental Data Set 1 online). However, monosaccharide levels were constitutively low in FD-Irp9 plants at NT and did not decrease further at HT.

Distinct Correlation Networks between SA and Phenylpropanoid Metabolites

A panel of 45 metabolites that exhibited altered abundance in response to temperature and/or SA manipulation, including those described above, was subjected to correlation analysis across all samples. Two distinct modules were identified, represented by SA-related metabolites and PGs/phenylpropanoids, respectively (Figure 5). The SA-related metabolites (denoted as group 1a in Figure 5) were positively correlated, via Phe as a key connector, with amino acids, TCA cycle intermediates, and sugar alcohols (group 1b) but negatively with most of the phenylpropanoids and soluble sugars (group 2). PGs, in general, showed positive correlations with other phenylpropanoids and soluble sugars, consistent with a coordinated synthesis utilizing both phenylpropanoid skeletons and hexoses from primary carbon pathways. The differential behaviors between chlorogenic acid isomers mentioned above were also captured in the correlation network. While 5-CQA was positively correlated with other phenylpropanoids in group 2, 3-CQA and 4-CQA were coregulated with SA metabolites in group 1a (Figure 5). Four other metabolites in group 1a also exhibited strong correlations

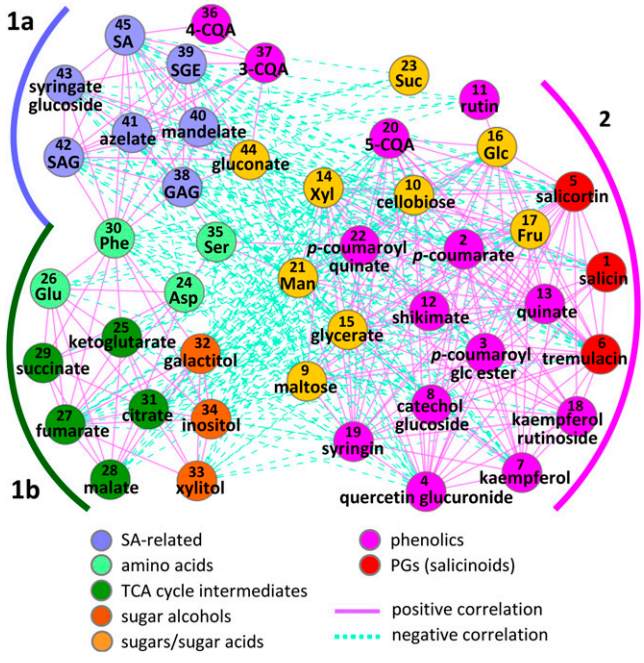

Figure 5. Metabolite Correlation Network in Response to SA and Temperature Manipulation.

Significant associations (absolute values of Pearson correlation coefficients ≥ 0.5, P ≤ 0.05) from all pairwise comparisons across all samples are visualized in Cytoscape. Compounds are numbered to facilitate cross-referencing with Figure 6 and Supplemental Data Set 1 online and color-coded by metabolite class.

with SA metabolites, and they accumulated preferentially in the FD-Irp9 lines. One was identified as putative syringic acid glucoside by HPLC–TOF/MS (see Supplemental Figure 1E and Supplemental Data Set 1 online). Its level was 10- to 50-fold higher in the FD-Irp9 lines and ~80% lower in the NahG lines compared with the wild type at NT. Two other metabolites were identified by GC-MS exclusively in FD-Irp9 samples (see Supplemental Data Set 1 online). One was related to mandelic acid, while the other was confirmed by authentic standard as the aliphatic signaling molecule azelaic acid (Jung et al., 2009). Gluconic acid was the only other structurally unrelated metabolite (besides azelaic acid) that correlated strongly with all SA metabolites. It was present in all plants but at significantly higher levels in the FD-Irp9 lines (see Supplemental Data Set 1 online). The nature of these compounds, ranging from phenolic acid and glucoside to fatty acid and hexonic acid, suggested that they have distinct origins, either as SA-derived or SA-stimulated metabolites.

Overlapping Metabolic Responses to SA and Heat Treatment

Hierarchical clustering analysis was performed to identify informative patterns of metabolic change among genotypes and/or treatments (Figure 6). Irp9 and NahG samples clustered with the wild type into two distinct branches according to temperature treatments (NT versus HT). The FD-Irp9 samples also formed temperature-dependent groups that clustered separately from the wild-type, Irp9, and NahG samples. Overall, HT triggered extensive metabolic changes in the wild-type, Irp9, and NahG plants, but the temperature-induced changes in FD-Irp9 lines were less striking. In fact, many metabolites in the FD-Irp9 plants under NT exhibited patterns that resembled those of HT-treated wild-type, Irp9, or NahG plants and included soluble sugars, PGs, 5-CQA, and other phenylpropanoids (corresponding to group 2 in Figures 5 and 6). Most of these metabolites showed decreased abundance in response to HT and/or high SA, consistent with their negative correlation with SA metabolites (Figure 5). Group 1b encompasses amino acids as well as the heat-responsive metabolites (TCA intermediates and sugar alcohols) mentioned above. Group 1a includes primarily SA-related metabolites with biased accumulation in the FD-Irp9 lines. Together, the metabolite results showed that SA hyperaccumulation led to a host of metabolic adjustments, involving primary and secondary metabolites, as well as antioxidants and potential signaling molecules.

SA-Mediated Transcriptome Responses Also Recapitulated Heat-Induced Responses

Microarray experiments were performed to gauge the transcriptional responses of young source leaves (LPI-5) to SA manipulation, using the wild type and one Irp9 (I6), one NahG (N31), and two FD-Irp9 (F10 and F52) transgenic lines with contrasting SA levels. Genes that were differentially expressed (DE) due to SA perturbation (transgenic versus wild-type) or temperature treatment (NT versus HT) were identified using adjusted P ≤ 0.05 and fold change ≥ 2 (see Methods).

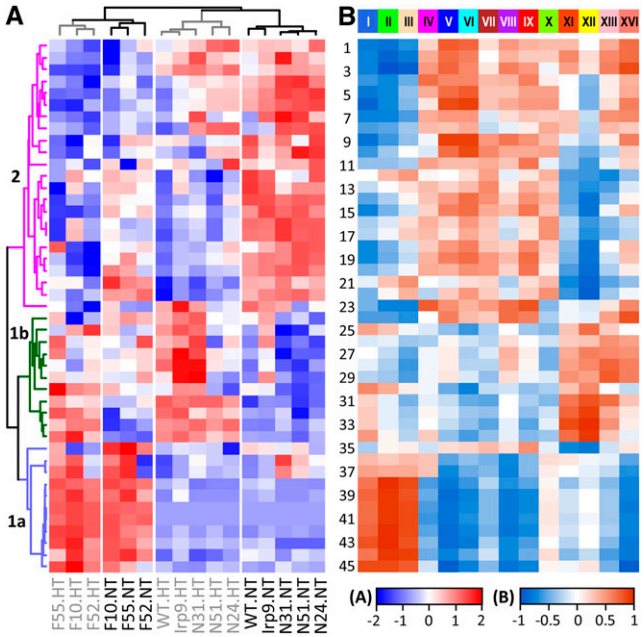

Figure 6. Metabolite and Gene Network Correlation.

(A) Hierarchical clustering analysis of relative metabolite abundance across genotypes and treatments. Metabolite numbering and grouping are the same as in Figure 5.

(B) Heat map illustration of correlations between metabolites and module eigengenes obtained from gene network analysis. Modules are shown on top. Scale bars depict the correlation strength and directionality (positive or negative) for both panels.

Compared with the wild type, I6 exhibited the fewest DE genes under either NT or HT (see Supplemental Figure 4 online), consistent with its overall metabolite profile similarity to the wild type. The numbers of DE genes were greater for N31 and F52, but the DE response was most conspicuous for the F10 line. The difference between F10 and F52 was in accordance with their SA levels and thus reflected a dose-dependent transcriptional response. At HT, the number of DE genes decreased in N31, but the number increased considerably in F52, approaching that of F10 (see Supplemental Figure 4 online). In general, more genes were upregulated than downregulated in all transgenics at NT, but DE patterns were more complex under HT.

Gene expression responses to HT in the different genotypes were summarized in a Venn diagram (Figure 7A). The I6 line was excluded for clarity of presentation because it was least affected metabolically and transcriptionally. Only a small number of genes showed significant differences in all genotypes, with 32 upregulated and seven downregulated (Figure 7A). Genes encoding heat shock proteins and vegetative storage proteins predominated in the upregulated group. Between 177 and 580 genes showed genotype-specific DE response to heat, and these genes were subjected to clustering analysis to identify representative expression patterns within each group (Figures 7B to 7G). Across genotypes, the vast majority of these genes responded similarly to HT (i.e., up- or downregulation), varying only in degree. For example, the largest cluster F included 236 genes that showed HT-reduced expression in all genotypes, but only the differential in the F10 line satisfied our DE criteria (Figure 7F). The transcript levels of many of these genes in unstressed FD-Irp9 plants resembled those in heat-treated wild type. Accordingly, we found considerable overlap between DE genes that were sensitive to SA (F10 versus the wild type) and to heat (NT versus HT in the wild type): ~40% of the heat-responsive DE genes in the wild type were similarly up- or downregulated by SA hyperaccumulation (Figure 7H). The results were consistent with findings from metabolite profiling and suggested that SA hyperaccumulation recapitulated the HT-induced transcriptional responses as well.

Gene Ontology (GO) enrichment analysis was performed to identify cellular functions that were overrepresented among SA- and/or heat-responsive genes. GO categories associated with biotic and abiotic stress responses and signal transduction were significantly overrepresented among genes that were upregulated in the FD-Irp9 lines, while genes related to photosynthesis and carbohydrate metabolism were overrepresented among those that were downregulated in these lines (see Supplemental Figure 5A online). Analysis of heat-responsive genes revealed two distinct clusters according to their expression patterns (up- versus downregulation), with high-SA (F10 and F52) and low-SA (wild-type, I6, and N31) lines forming separate subgroups within each cluster (see Supplemental Figure 5B online). GO categories associated with oxidative stress responses, redox homeostasis, and protein folding were overrepresented among heat-stimulated genes. Genes associated with polysaccharide and phenylpropanoid metabolism were repressed by heat, especially in

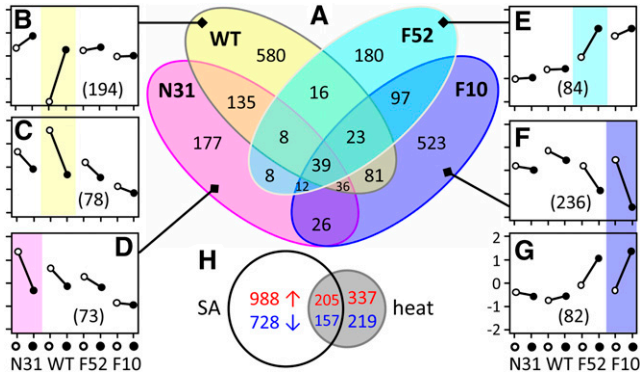

Figure 7. Gene Expression Responses to Heat Treatment in Wild-Type and Transgenic Lines.

(A) Venn diagram of genes significantly affected by heat in the four genotypes. WT, the wild type.

(B) to **(G)** Representative patterns of gene expression profiles based on clustering analysis of gene subsets from **(A)**. The average expression profiles of the four genotypes are shown in each panel, with gene number listed in parentheses. Genes exhibiting significant differences are shaded by genotype according to the Venn diagram in **(A)**. Open and filled circles denote normal and high temperature treatments, respectively. *y* axis in **(G)** is for **(B)** to **(G)**.

(H) Venn diagram of genes significantly changed in F10 relative to the wild type (SA effect) or by heat treatment in the wild type (heat effect).

[See online article for color version of this figure.]

low-SA lines (see Supplemental Figure 5B online), consistent with findings from the metabolite analysis.

Weighted Correlation Network Analysis Identified SA-Regulated Gene Modules

Transcriptional interactions of SA- and/or heat-sensitive genes were investigated using the eigengene weighted correlation network approach (Langfelder and Horvath, 2008). A less stringent procedure (see Methods) was used to obtain 8570 DE genes, which included the two bacterial transgenes, *Irp9* and *NahG*. We also added the marker metabolite SAG as a nongene node (using normalized relative abundance of corresponding samples) in order to facilitate identification of genes correlating with SA changes. The degree distribution of the resultant network follows the power law (see Supplemental Figure 6A online), a common property of scale-free networks (Barabási and Albert, 1999). Fourteen coregulation modules were identified, and the expression profile of each module is represented by the module eigengene (first principal component) (see Supplemental Figure 6 online). Correlation analysis of module eigengenes with metabolite traits across genotypes and treatments allowed identification of covarying gene-metabolite responses (Figure 6). For instance, SA-related metabolites (group Ia) showed strong positive correlations with the royal blue (I), green (II), and tan (III) modules of the network but were negatively correlated with the blue (V) and cyan (VI) modules (Figure 6). Specifically, genes in the green (II) module exhibited an SA-dependent expression profile, lowest in N31 and highest in F10 (see Supplemental Figure 6C online), and not surprisingly, both the SAG and *Irp9* nodes were captured in this module. PGs (metabolite Nos. 1, 5, and 6 in Figure 6) were found to correlate positively with the blue (V) and cyan (VI) modules but negatively with the royal blue (I) and green (II) modules, in accordance with the inverse relationship between PGs and SA metabolites described above. The yellow (XII) module exhibited a temperature-dependent regulation regardless of genotype (see Supplemental Figure 6J online). GO enrichment analysis provided further support for differential functional associations of the various modules (see Supplemental Table 2 online). For example, genes associated with defense response and signal transduction were greatly enriched in the SAG-containing green (II) module. Genes associated with heat response and protein folding were enriched in the yellow (XII) module, consistent with their transcriptional induction by heat.

Research in biological networks has shown that highly connected nodes (hubs) are usually enriched with genes that play important roles in governing the behavior of the system under investigation (Jeong et al., 2001; Carter et al., 2004). To identify key players in our reconstructed network, genes were ranked based on their total connectivity (k) in the network, and the top 5% most densely connected nodes were designated as hubs (Basso et al., 2005). The k of the hub genes ranged from 162.3 to 314.7, severalfold greater than the average (31.1) or median (49.1) k of all nodes in the weighted network. Collectively, these hubs participated in nearly half of the total connections (45,501 of 97,162 edges) in the network, with an average of 103 connections per hub gene. When the gene network was visualized in Cytoscape (Figure 8A), these hubs were found in a localized cluster (Figure 8B), in sharp contrast with the more scattered distribution of the top 5% nodes from each module (Figure 8C). More than 75% of the hubs, including SAG, were from the green module (Table 1), suggesting that SA-responsive genes were drivers of the network. To confirm this observation, and to further explore the effects of SA hyperaccumulation on gene network rewiring, we divided the data into wild-type-like (the wild type, I6, and N31) and high-SA (F10 and F52) groups and constructed two subnetworks (hereafter, referred to as wild-type and FD-Irp9 subnetworks, respectively) for comparative analysis. The two subnetworks appeared quite distinct, with little conservation across modules (see Supplemental Figures 7A to 7C online). When compared against the total network, an overall greater degree of module conservation was observed with the

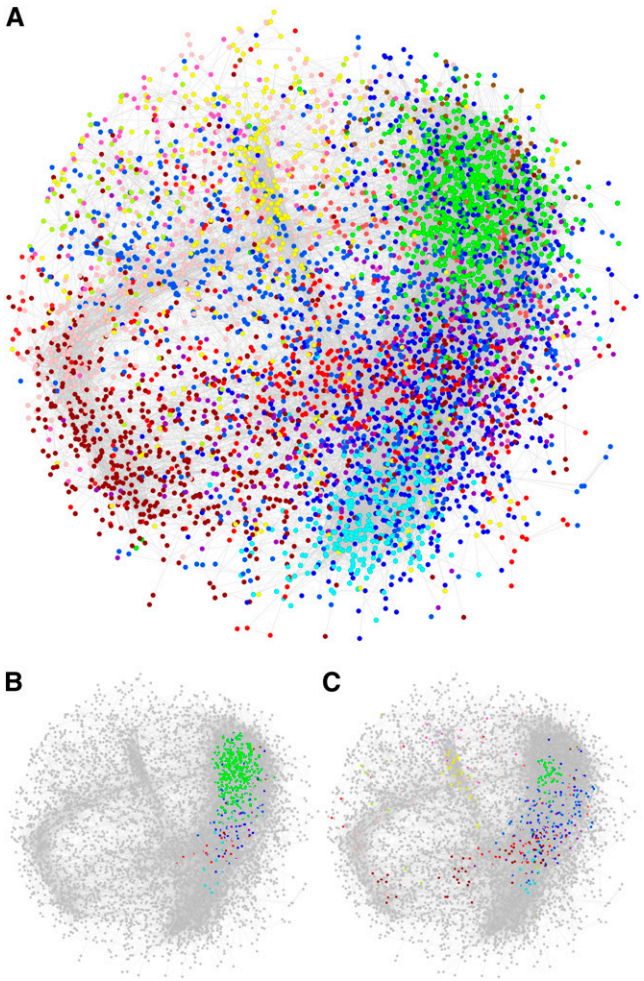

Figure 8. Topology of the Weighted Gene Correlation Network.

(A) The inferred gene network. Nodes are colored according to their module assignment.

(B) Distribution of the top 5% most highly connected hub genes from the entire network.

(C) Distribution of the top 5% most connected nodes from each module. Non-hub nodes in **(B)** and **(C)** are shown in gray.

Table 1. Module Assignment of Hub Genes from the Total as Well as FD-Irp9 and Wild-Type Subnetworks.

Module[a]	Node No.	Total Network	FD-Irp9 Subnetwork	Wild-Type Subnetwork	Differential Connectivity ($k_{FD\text{-}Irp9} - k_{WT}$)	
					k Gain	*k* Loss
Royal blue (I)	1640	25	127	25	136	24
Green (II)	932	330	55	4	60	7
Blue (V)	1235	38	118	7	144	14
Cyan (VI)	346	14	21	22	10	9
Brown (VII)	1179	4	11	160	5	201
Red (IX)	493	14	13	9	11	5
Yellow (XII)	746	0	21	54	6	41
Pink (XIII)	665	0	19	144	2	119
Total[b]	8751	438	438	438	438	438

[a]Only eight modules are shown.
[b]The numbers are summed from all modules.

wild type than with the FD-Irp9 subnetwork (see Supplemental Figures 7D and 7E online). However, the hub genes from the total network were more similar to those from the FD-Irp9 subnetwork than from the wild-type subnetwork (see Supplemental Figures 7F to 7H online), suggesting that the relatively small number of hub genes contributed significantly to SA-modulated network rewiring.

Analysis of differential connectivity between the two subnetworks (determined as $k_{FD\text{-}Irp9} - k_{WT}$) showed that the top 5% nodes that gained connectivity (i.e., with more coregulating genes) in the FD-Irp9 subnetwork overlapped substantially (~70%) with the hub genes there. These genes corresponded primarily to the SA-correlated royal blue (I), green (II), and blue (V) modules in the total network (Table 1). Conversely, a majority of hub genes (~55%) in the wild-type network lost their connectivity in the FD-Irp9 network (Table 1). Using an arbitrary differential connectivity cutoff of 100 and a DE (fold change) cutoff of ≥4 between the two plant groups, a total of 144 genes (plus the SAG node) showed increased expression as well as increased connectivity in the FD-Irp9 plants, 80% of which were from the green (II) module (Figure 9A, top right corner). These genes thus represent potential drivers contributing to the widespread transcriptomic changes, involving both differential expression as well as altered network connectivity, due to SA hyperaccumulation.

Potential Drivers of the SA-Modulated Network

The group of 144 potential drivers was enriched with receptor-like protein kinases (*RLKs*) and various transporters, oxidoreductases, and transcription factors, most of which (~73%) were also hubs in the total network (see Supplemental Data Set 2 online). *RLKs* belong to the protein kinase superfamily with important functions in defense signaling (Morris and Walker, 2003; Lehti-Shiu and Shiu, 2012). Of the 308 *RLKs* captured in our network (i.e., with differential expression among genotypes or treatments), a majority of them (~77%) were associated with SA-correlated modules, especially the green (II) module where *RLKs* accounted for ~13% (132) of its nodes. The large number of *RLKs* with increased expression as well as increased network connectivity in high-SA poplars suggested that they have roles in the reprogramming of signaling pathways in these plants. The group of oxidoreductases included the entire *Populus* NUCLEOREDOXIN1 (NRX1) subfamily, which is the only family of small redox proteins (glutaredoxins or thioredoxins [TRXs]) represented among the drivers (see Supplemental Data Set 2 online). All nine *NRX1* probes on the microarray exhibited an SA-dependent expression pattern that was also confirmed by qRT-PCR (Figure 10; see Supplemental Table 3 online for gene model correspondence). Their involvement in SA network rewiring represents a previously undescribed role of plant NRX1 in stress-associated redox regulation. Among the 144 drivers were orthologs of *Arabidopsis* genes that are known to be involved in the SA defense signaling pathway. Examples include orthologs (POPTR_0014s03260 and POPTR_0019s03090) of patatin-like phospholipase A_2 (Scherer et al., 2010) and several defense-associated *WRKY* transcription factors (Xu et al., 2006; Terpstra et al., 2010) that exhibited SA-stimulated expression in our study. The observed transcriptional responses of representative *RLK* (Poptr_0012s01760 and Poptr_0017s09520) and *WRKY* (Poptr_0006s27950 and Poptr_0016s14490) genes were confirmed by qRT-PCR (see Supplemental Figure 8 online). Overall, the network analysis provided a glimpse of previously reported as well as new SA-sensitive components of redox regulation and inducible defense signaling pathways.

Because SA-hyperaccumulating poplar exhibited constitutive metabolic and transcriptional responses that resembled those of heat-treated poplars, we reasoned that the group of potential drivers may modulate the general oxidative stress responses of *Populus*. To find support for this hypothesis, we examined published *Populus* leaf microarray data sets derived from oxidative stress experiments. The analysis encompassed 48 paired comparisons (stressed versus unstressed samples) of drought (Wilkins et al., 2009; Cohen et al., 2010; Hamanishi et al., 2010; Raj et al., 2011; Chen et al., 2013), wounding (Yuan et al., 2009), pathogen (Azaiez et al., 2009), and ozone responses (Street et al., 2011). After quality control filtering, DE of the 144 driver genes, when present, was assessed by fold change and P values (see Methods) and shown in box-and-whisker plots for all

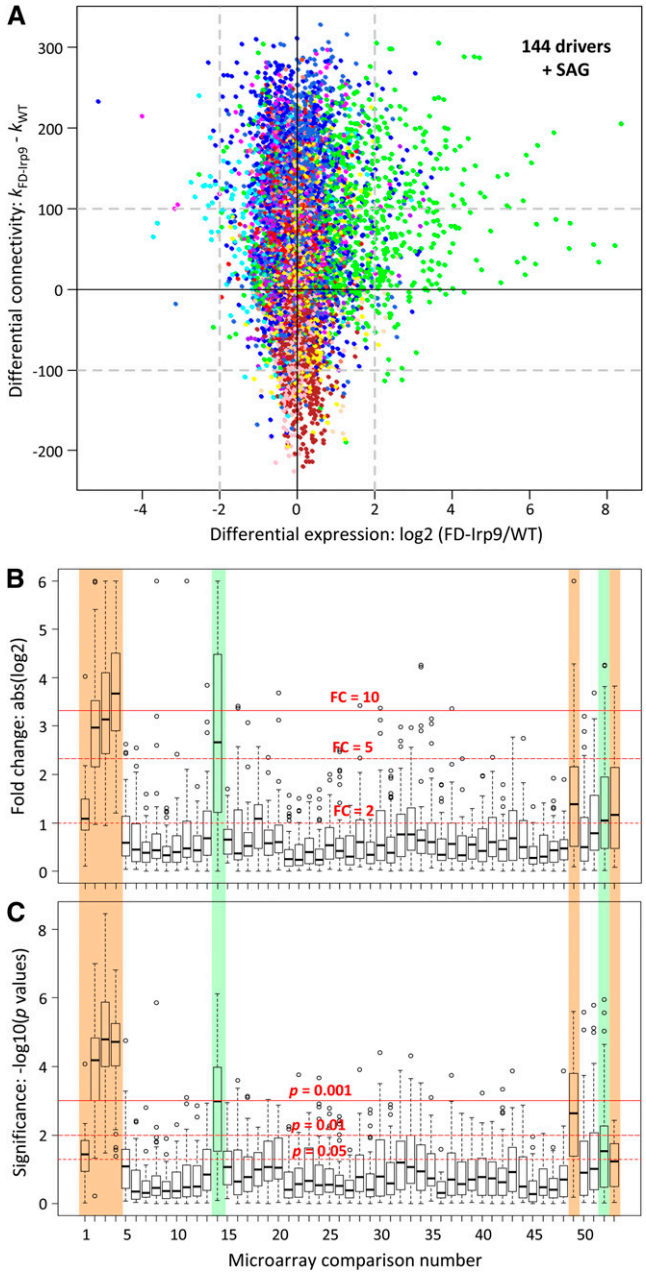

Figure 9. Graphic Representation of Potential Drivers in the SA-Modulated Gene Network.

(A) Scatterplot of differential expression and differential connectivity between the wild-type (WT) and FD-Irp9 subnetworks. Nodes are colored by their module assignment in the total network. Dashed lines denote the arbitrary cutoffs for the two parameters. Potential drivers that exhibited increased expression and increased network connectivity in the FD-Irp9 plants relative to the wild type are found on the top right corner (144 genes plus the SAG node).

(B) and **(C)** Expression responsiveness of the driver genes to oxidative stress treatments based on meta-analysis of published *Populus* leaf microarray data. Gene expression differences between stressed samples and their respective controls were assessed by fold change (FC; **[B]**) or statistical significance (P value; **[C]**). Horizontal red lines depict three arbitrary thresholds in each panel. Stress experiments that triggered significant changes in driver gene expression are shaded in color and include SA and/or heat (Nos. 1 to 4; this study), wounding (No. 14), drought (No. 49), pathogen infection (No. 52), and ozone (No. 53). See Supplemental Table 4 online for the complete list of comparisons and data source.

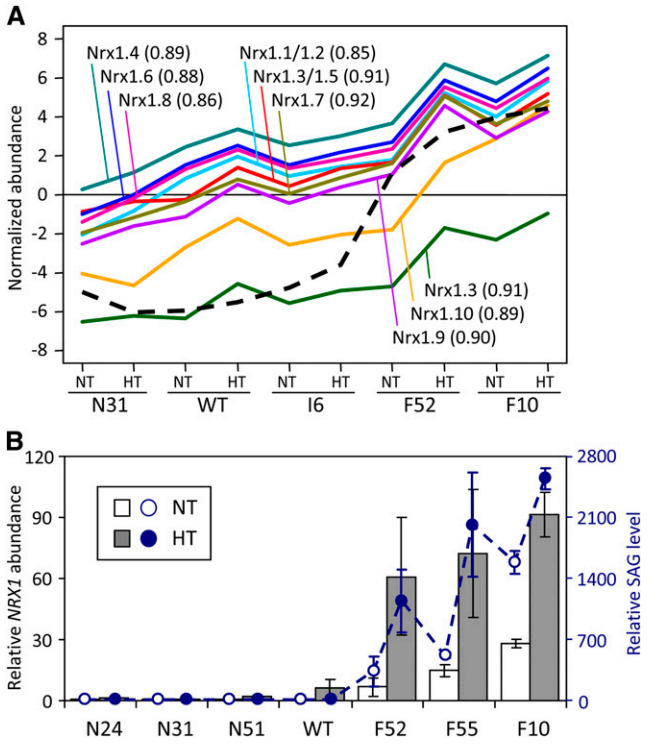

Figure 10. SAG and *NRX1* Transcript Abundance.

(A) Microarray hybridization signals of *NRX1* probes (solid lines) correlated with SAG abundance (dashed line) across genotypes and treatments. Only the best-matching *NRX1* name is shown for each probe (see Supplemental Table 3 online for gene model correspondence and probe gene sequence identity matrix for potential cross-hybridization). The Pearson correlation coefficient between SAG and the respective *NRX1* probe is shown in parentheses. WT, the wild type.

(B) Relative *NRX1* transcript abundance obtained by qRT-PCR (vertical bars) superimposed over SAG levels (dashed line). The *NRX1* transcript levels (left axis) are shown as means ± SD of two to three biological replicates. The primers were designed based on consensus sequence of all *Populus NRX1* members. SAG data (right axis) are from Figure 4.

[See online article for color version of this figure.]

sample pairs (Figures 9B and 9C; see Supplemental Table 4 online). Data from this study were included as reference. As expected, expression of these driver genes showed significant and large fold change differences due to elevated SA (Nos. 1 to 4, Figures 9B and 9C). The responses followed an SA dose-dependent trend: stronger in F10 (Nos. 3 and 4) than F52 (Nos. 1 and 2), and at HT (Nos. 2 and 4) than NT (Nos. 1 and 3). These genes also responded strongly to wounding (No. 14), drought (No. 49), pathogen (No. 52), and ozone (No. 53, Figures 9B and 9C), sometimes in a dose-dependent manner (see Supplemental Table 4 online for explanations). Specifically, of the large number of drought samples analyzed, a significant response of the driver genes was observed only in *Populus simonii* (No. 49), a hardy species indigenous to northern China (Wang et al., 2012). Similar results were obtained for the 438 network hub genes, but the overall responses were weaker than those of the driver genes (see Supplemental Figure 9 online), consistent with greater responsiveness of the driver genes. A common theme among the biotic (pathogen) and abiotic (drought, wounding, and ozone) stressors is their ability to trigger oxidative responses in plants (Kovtun et al., 2000). We interpret the results to suggest that elevated oxidative state, due either to genetic variation, SA overproduction, or stress manipulation, primes plants to elicit potent oxidative responses as evidenced by elevated expression of the driver genes. Thus, this analysis provided independent support for the involvement of the driver genes in poplar oxidative stress responses, including those induced by elevated SA.

DISCUSSION

Metabolic and Transcriptome Reprogramming in High-SA Poplar Resembles That Induced by Oxidative Stress

Our results provide multiple lines of evidence to support a direct role of SA in eliciting sustained oxidative responses. Constitutively elevated SA promoted transcriptional and metabolic changes in transgenic FD-Irp9 lines that resembled those observed in wild-type and wild-type-like (Irp9 and NahG) plants after prolonged growth at HT, a condition known to increase oxidative stress (Kaplan et al., 2004; Caldana et al., 2011). In particular, there was substantial overlap between HT and SA upregulated genes, with both groups showing similar GO enrichment in oxidative stress responses. While stress metabolite sugar alcohols were increased by HT regardless of genotype, the abundance of Glc, Fru, and many of the phenylpropanoids were constitutively low in leaves of FD-Irp9 plants, similar to levels that were observed in heat-treated wild-type or wild-type-like poplars.

Of particular interest was the strong correlation of azelaic acid and gluconic acid with SA and SA conjugates. Azelaic acid was recently proposed to be a mobile signal in *Arabidopsis* SAR, accumulating in phloem exudates and priming plants to induce SA production in response to pathogen attack (Jung et al., 2009). These authors showed that azelaic acid accrual was dependent on pathogen-induced SA synthesis, and it in turn augmented SA production for defense (Jung et al., 2009). Another study suggested that azelaic acid is derived from radical-catalyzed peroxidation and fragmentation of plastid lipids as a general oxidative stress response (Zoeller et al., 2012). The preferential detection of azelaic acid in FD-Irp9 poplars and its strong correlation with SA metabolites in response to HT are in support of a direct relationship between SA and azelaic acid (Jung et al., 2009) and of the view that azelaic acid represents an oxidative stress marker (Zoeller et al., 2012). The biosynthesis and metabolism of gluconic acid is poorly understood in plants, but in microbes and fungi, gluconic acid along with H_2O_2 is derived from oxidation of Glc (Ramachandran et al., 2006). Although Glc oxidase homologs have not been identified in plants, several proteins of the berberine bridge enzyme family exhibit carbohydrate oxidase activities (Carter and Thornburg, 2004; Custers et al., 2004), some with SA- and pathogen-inducible expression (Custers et al., 2004). Overexpression of Glc oxidase of either fungal or plant origin led to elevated H_2O_2 production

and enhanced disease resistance (Wu et al., 1995; Custers et al., 2004), consistent with a link between gluconic acid (via H_2O_2) and defense.

Changes in Chlorogenic Acid Metabolism May Provide Protection to Chloroplasts during SA-Induced Stomatal Closure

We observed that the increases in net photosynthesis and transpiration due to HT were attenuated in lines with constitutively elevated SA (Figure 2). In addition, stomatal conductance was clearly reduced in FD-Irp9 lines at HT, when SA and SAG levels were further increased (Figure 4). This is consistent with the interpretation that SA induced partial stomatal closure as has been reported in several species (Lee, 1998; Mori et al., 2001; Khokon et al., 2011). Stomatal closure can lead to photosynthetic electron transport overload and greater production of ROS in the light (Asada, 2006). This, along with elevated levels of SA metabolites (including azelaic acid and gluconic acid), presumably intensified the oxidative state of the FD-Irp9 plants at HT. Therefore, during HT growth, reduced photosynthetic capacity, increased glycosylation of SA, and elevated oxidative state in the growth-sustained FD-Irp9 plants may have exacerbated a metabolic trade-off at the expense of soluble phenylpropanoids/sugars. Interestingly, chlorogenic acid isomers 3-CQA and 4-CQA were the only phenylpropanoids from the panel that showed positive correlations with SA metabolites, while 5-CQA was coregulated with other phenylpropanoids (Figure 5). Chlorogenic acid isomerization is known to be sensitive to developmental or environmental cues (Joët et al., 2010). Given the reported close association of chlorogenic acids with chloroplasts in young leaves (Mondolot et al., 2006) and their importance as antioxidants (Nakatani et al., 2000; Niggeweg et al., 2004), we posit that the changes in chlorogenic acid pool composition reflect a change in cellular redox due to elevated SA and/or SA-induced stomatal closure. The fact that chlorogenic acids are abundant in *Populus* leaves suggests a readily available and SA-sensitive pool for local protective responses, perhaps at the subcellular level, in the event of SA-mediated changes in ROS.

Redox Regulation Pathways Differ between *Populus* and *Arabidopsis*

The correlation network analysis enabled identification of potential drivers in SA-modulated rewiring of the transcriptional network. Meta-analysis of the *Populus* leaf stress transcriptome showed that these driver genes were also highly responsive to a host of biotic and abiotic oxidative stressors (Figures 9B and 9C). The most prominent group was RLKs that have been implicated in a wide range of signaling cascades during plant growth, development, and biotic and abiotic responses (Morris and Walker, 2003; Afzal et al., 2008; Lehti-Shiu et al., 2009). The large number of *RLKs* with increased expression as well as increased network connectivity in high-SA poplars is consistent with the reported activation of several *Arabidopsis RLKs* upon oxidative stress or SA treatment (Czernic et al., 1999; Ohtake et al., 2000). Oxidoreductases were also enriched among the drivers in accordance with their importance to redox regulation in stress response and SA signaling (Foyer and Noctor, 2005). *NRX1s* were the only *TRX/GRX* genes that exhibited SA-dependent expression and network rewiring in this study. NRX1 has not been characterized in *Arabidopsis* where SA-mediated defense signaling depends on the TRX-h subfamily (i.e., TRXh3 and TRXh5 paralogs) for redox changes (Tada et al., 2008). Interestingly, *Populus* lacks apparent orthologs of the *Arabidopsis TRXh3/5* duplicate, in sharp contrast with its tandem amplification of *NRX1s* relative to the single-copy *Arabidopsis NRX1* (Chibani et al., 2009). We interpret these observations to suggest that there are distinct redox regulation mechanisms associated with SA signaling in *Populus* and *Arabidopsis*. This interpretation is also consistent with the absence in the reconstructed *Populus* correlation network of *NON-EXPRESSOR OF PATHOGENESIS-RELATED GENES1* (*NPR1*), which in *Arabidopsis* is a key regulator of the SA-mediated SAR response (Cao et al., 1997). The *Populus NPR1* ortholog (POPTR_0006s15040) was poorly expressed in leaves and insensitive to SA (no significant differences between the wild type and transgenics). The predicted POPTR_0006s15040 protein lacks the key Cys residues implicated in redox-mediated nuclear translocation (Cys-156; Tada et al., 2008) or SA interaction (Cys-521/529; Wu et al., 2012) for defense. The data suggested that whereas some aspects of the SA signaling pathway appear to be conserved between *Populus* and *Arabidopsis*, other components have diverged during evolution.

The contrasts in SA signaling are accompanied by differences between *Populus* and *Arabidopsis* in their homeostatic regulation of SA. First, constitutive levels of SA in *Populus* are substantially higher than those in *Arabidopsis* (Koch et al., 2000). Second, whereas twofold to 200-fold total SA increases in *Arabidopsis* negatively affect growth (Rivas-San Vicente and Plasencia, 2011), multifold differences in total SA levels are frequently observed among *Populus* genotypes (Koch et al., 2000; Vahala et al., 2003; Diara et al., 2005). As reported here, total SA increases of up to 1000-fold in transgenic *Populus* had no apparent effects on plant growth. This finding along with a similar one reported for transgenic tobacco (*Nicotiana tabacum*) (Verberne et al., 2000) suggested that the negative effect of elevated SA on *Arabidopsis* growth is not universal in plants. Third, *NahG*-expressing transgenic *Arabidopsis* is unable to accumulate SA and SAG, resulting in increased susceptibility to pathogens and abiotic stresses, including heat (Delaney et al., 1994; Rao and Davis, 1999; Larkindale and Knight, 2002). However, sustained accumulation of SA and/or SAG in *NahG* poplars, along with significant increases of SA breakdown product catechol glucoside, was reported in two independent studies (Morse et al., 2007; this study). This is consistent with great metabolic flexibility and a capability for high rates of SA biosynthesis and metabolism in poplars. SA appears to be more integrated with a versatile chemical defense system of poplars that is largely constitutive. In response to stressors such as heat or ozone that are oxidative, SA may mediate stomatal closure along with changes in antioxidant capacity of large preexisting phenylpropanoid pools for defense.

In summary, we observed that endogenously elevated SA in *Populus* elicited potent and sustained oxidative responses. Stomatal behavior was altered as was transcriptional and

metabolic programming. The high photosynthetic capacity of *Populus* and the metabolic flexibility afforded by the dynamic chlorogenic acids pool are both likely to contribute to SA tolerance. Several genes and metabolites identified from our correlation analyses offer new insights into the coordination of as yet largely unexplored metabolic and transcriptional networks that may underpin the capacity of certain *Populus* genotypes to tolerate oxidative stressors, including drought, ozone, and salinity.

METHODS

Generation of Transgenic *Populus*

The *Yersinia enterocolitica Irp9* gene was PCR amplified from plasmid pTIrp9 (Pelludat et al., 2003) with primers that introduced 5′-*Sal*I or *Bgl*II and 3′-*Nhe*I sites (see Supplemental Table 5 online), TOPO-TA cloned into pCR2.1 (Invitrogen), and sequence verified to produce pCR-Irp9a and pCR-Irp9b, respectively. The chloroplast transient peptide sequence from *Arabidopsis thaliana FD2* gene (At1g60950) was PCR amplified with 5′-*Bgl*II and 3′-*Sal*I sites and inserted in frame upstream of pCR-Irp9a to generate pCR-FD-Irp9 and sequence-confirmed. The Irp9 or FD-Irp9 fragments were then subcloned into pCambia1302 at *Bgl*II and *Nhe*I sites downstream of the 35S promoter to generate the respective binary constructs. The *NahG* construct in pCIB200 (Gaffney et al., 1993) was provided by Syngenta Biotechnology. Transformation of *Populus tremula* × *alba* clone 717-1B4 was performed as described (Meilan and Ma, 2006). Primary transformants were transplanted to soil and maintained in a greenhouse for initial characterization. Selected transgenic lines along with the wild type were vegetatively propagated by rooted cuttings as described (Frost et al., 2012) for subsequent experiments.

Heat Experiments

Two heat experiments were conducted. One experiment was designed to monitor photosynthetic responses to temperature variations in a growth chamber. Vegetatively propagated wild-type and two transgenic lines each of FD-Irp9 (F52 and F55) and NahG (N24 and N31) plants were grown under NT (27°/17°C, day/night) until they reached ~140 cm in height. After initial (prestress) photosynthesis measurements, the chamber setting was changed to HT (35°/25°C, day/night) for 10 d before returning to NT for recovery. Net photosynthesis, stomatal conductance, and transpiration rates were measured three times during the 10-d HT period and once after 1-week recovery. Two leaves (LPI-5 and LPI-10) were measured independently on each plant using a LiCor LI-6400XS at a saturating light intensity of 1500 μmol/m^2/s as described (Frost et al., 2012). To test the effects of HT treatment, genotype, and their interaction on photosynthesis, data were analyzed by repeated measures ANOVA, using a linear mixed effect model with the lme function in *R*. Significant genotypic differences were further analyzed by pairwise comparisons between the wild type and each transgenic line.

The other heat experiment was designed for comparative analyses of plant growth, electrolyte leakage, gene expression, and metabolite response under different temperature regimes. The wild type and two to three lines each of the Irp9 (I6 and I8), FD-Irp9 (F10, F52, and F55), and NahG (N24, N31, and N51) transgenics were used. Vegetatively propagated plants were randomly assigned to two identical growth chambers and grown to a height of ~120 cm under NT. At that time, plants in one chamber were subjected to HT, while the other chamber was maintained at NT. One week after the HT treatment commenced, leaf discs from LPI-6 were collected for electrolyte leakage assays and LPI-1 and LPI-5 were snap-frozen in liquid nitrogen for gene expression and metabolite analyses. After sampling, the treatment chamber was reset to NT for recovery, and samples were collected again 1 week later. All sampling was conducted in the light during mid-day and under the specified chamber temperature (NT or HT).

Plant Growth

Plant height growth was monitored in the two-chamber heat experiment from September to November of 2010. Because initial plant sizes varied, and because height growth was approximately linear during the monitoring period for all plants, height increment per unit time was used for statistical analysis by repeated measures ANOVA. Height and diameter growth were also monitored using a separate cohort of plants in a greenhouse experiment during June, 2011. Evaporative cooling was used to maintain greenhouse temperature of ~5°C below daytime ambient temperatures, which ranged from 33 to 37°C maximum during this time. Genotypic differences of growth rate were tested by repeated measures ANOVA.

Electrolyte Leakage Analysis

Two 6-mm leaf discs (LPI-6) per plant were collected into 5 mL double-distilled water during tissue harvesting of the heat experiment and kept on ice in the dark for up to 4 h. Upon returning to the lab, the samples were incubated at ambient temperature under light for 6 to 7 h with gentle shaking. The incubation time was chosen based on preliminary testing that the electrolyte leakage reached a plateau by this time. Conductivity was measured using a Traceable conductivity meter. The samples were then boiled for 30 min and cooled to room temperature overnight before measurements were taken again. Blank (double-distilled water)-corrected conductivity values were used for statistical analysis by Student's *t* test. To evaluate temperature-dependent electrolyte leakage, leaf discs from LPI-5 of greenhouse-grown wild-type and F10 plants were randomly distributed into three tubes (five discs per tube with 10 mL double-distilled water). The tubes were incubated at 25, 37, and 50°C, and electroconductivity was monitored for 4 h. The samples were then boiled for 30 min to release total electrolytes. Measurements for the 37°C, 50°C, and boiled samples were taken after cooling to room temperature. Blank-corrected conductivity values were used for statistical analysis by repeated measures ANOVA.

Metabolite Profiling and Data Analysis

For initial transgenic plant screening, freeze-dried leaf powder (5 mg) was extracted in 500 μL methanol containing $^{13}C_6$-cinnamic acid, D_5-benzoic acid, and resorcinol as internal standards by sonication in ice water for 5 min. Following centrifugation, the extracts were stored at −80°C until HPLC analysis. For the heat experiments, freeze-dried leaf powder (10 mg) was extracted twice in 670 μL methanol:water:chloroform (46:30:24) containing $^{13}C_6$-cinnamic acid, D_5-benzoic acid, resorcinol, 2-methoxybenzoic acid, and adonitol as internal standards. Following vortexing and incubation at 70°C for 5 min (first extraction) and sonication in ice water for 15 min (second extraction), the aqueous phase from both extractions was combined. A fraction of the extract (700 μL) was evaporated to dryness in a CentriVap (Labconco) and the rest saved for HPLC analysis. Dried aliquots were resuspended in 40% methanol and further partitioned into relatively polar and nonpolar fractions using Advanta resin (Applied Separations) for GC-MS analysis as described (Jeong et al., 2004; Frost et al., 2012). Mass spectral data were processed by AnalyzerPro (SpectralWorks) for deconvolution and matching against the NIST08 (Babushok et al., 2007), FiehnLib (Kind et al., 2009; Agilent), and in-house authentic standard mass spectral libraries. The output files were then processed by a custom Web-based pipeline, MetaLab, for compound matching between samples based on retention index and mass spectral

similarity, followed by manual curation. The compiled data is shown in Supplemental Data Set 1 online, with the original data sets available at the MetaLab website (http://aspendb.uga.edu/) under analysis IDs 70, 71, 128, and 353.

Phenolic compounds were analyzed on an Agilent 1200 HPLC equipped with a diode array detector and a 6220 accurate mass time-of-flight mass spectrometer with dual electrospray ionization, using a ZORBAX Rapid Resolution Eclipse XDB-C18 column (4.6 × 50 mm, 1.8 μm; Agilent) and mobile phase solvents water:acetonitrile:formic acid = 97:3:0.1 (A) and 3:97:0.1 (B). The elution gradient was 3% B from 0 to 1 min, linear gradient to 17% B over 2 min, isocratic at 17% B for 2 min, linear gradient to 60% B over 4 min, and then to 98% B over 2 min, at a flow rate of 1 mL/min. Diode array detection was set at 260, 270, 280, 310, and 350 nm, and mass spectrometry acquisition at mass-to-charge ratio 100 to 1500 in negative electrospray ionization mode with the following parameters: gas temperature, 350°C; drying gas flow, 13 l/min; nebulizer pressure, 60 psig; capillary voltage, 3500 V; and fragmentor voltage, 125 V. Data were processed by MassHunter Qualitative Analysis, Mass Profiler, and MassHunter Quantitative Analysis software suite (Agilent), followed by manual curation. Metabolite identity was confirmed by authentic standards when possible or by searching the predicted mass-to-charge ratio and molecular formula against the KNApSAcK database (Afendi et al., 2012). SAG and GAG peaks were isolated using a fraction collector and treated with β-glucosidase. Aglycone identity was confirmed by comparison with authentic standards.

Relative abundance was determined as peak area of each metabolite divided by that of the internal standard (2-methoxybenzoic acid for GC polar, adonitol for GC nonpolar, and D_5-benzoic acid for HPLC metabolites), followed by a correction for differences in tissue dry weight. Metabolites that were significantly changed by HT or transgenic manipulation (P value ≤ 0.1 by Student's *t* test) were subjected to clustering analysis. The data were normalized by compound using the Z-score method, and clustering was performed using *R* function Heatmap.2 with the Pearson distance metrics and the average linkage method. To visualize metabolite correlations in a network context, the Pearson correlation coefficient was calculated for all metabolite pairs. Significant associations (absolute Pearson correlation coefficient ≥ 0.5, P ≤ 0.05) were visualized in Cytoscape v2.8.2 (Smoot et al., 2011).

Microarray Design, Hybridization, and Data Analysis

A new Agilent Poplar array (v2) was designed based on the JGI *Populus* genome release v2.2 for the 8x60K array platform. The coding sequence region was targeted for probe design, since the 3′-untranslated region is less conserved, sometimes with indels, among *Populus* species (Tsai et al., 2011b). Coding sequences were first BLAST searched against one another to remove highly similar sequences from different gene models. A series of probes was then designed using eArray (Agilent), and custom Perl scripts were used to evaluate probe specificity. A total of 43,070 probes were selected for the 40,330 predicted v2.2 gene models, more than 96% of which (38,770) were represented by specific probes (no other matches with ≥90% identity). We also included 12,080 probes designed for mRNA sequences that had poor or no matches in the v2.2 genome, in addition to 1160 probes for microRNAs and 295 probes for mitochondrial or chloroplastic gene models. Probes corresponding to the *Irp9* and *NahG* transgenes, as well as several reporter or selectable marker genes commonly used in transgenic research were also included.

RNA for microarray analysis was extracted from LPI-5 using the CTAB method (Tsai et al., 2011a) and treated with the Turbo DNA-free kit (Ambion) to remove genomic DNA. Two biological replicates were included for each genotype. cRNA target labeling was performed as described (Syed and Threadgill, 2006) using the One-color Quick Amp Labeling Kit (Agilent). Array hybridization and washing were performed with Agilent reagents and instructions. Arrays were scanned at 3-μm resolution and images processed using Feature Extraction v10.5.1.1 (Agilent). Intensity data were normalized by 75th percentile shift using GeneSpring GX11. Probes with low expression values (≤300 in all samples) were excluded, leaving 21,313 probes for further analysis.

DE was assessed using Limma (Smyth, 2005) and SLIM (Wang et al., 2011) packages, unless otherwise specified. SLIM uses P values obtained from Limma and applies a sliding linear model to estimate π_0 for a robust control of false discovery rate in multiple hypothesis testing. The significance threshold was fold change ≥2 and SLIM p_{max} = 0.05. GO enrichment analysis was conducted using *R* package topGO (Alexa et al., 2006), with GO annotation obtained from agriGO (Du et al., 2010) and *Arabidopsis* GO Slim (The Arabidopsis Information Resource). Significance of enrichment was determined by Fisher's exact test, and the negative $\log_{10}$ transformed P values were used for visualization in heat maps. To reduce redundancy, semantic similarity among GO terms was computed using GOSemSim (Yu et al., 2010), followed by cutting the hierarchical tree of GO categories into clusters. Representative GOs from the clusters, typically those with lower P values and/or higher GO hierarchy levels, were selected for visualization.

Gene Network Construction and Visualization

Coexpression networks were constructed using the WGCNA (v1.18.1) package in *R* (Langfelder and Horvath, 2008). DE genes were obtained with a less stringent cutoff (ANOVA P ≤ 0.05 and fold change ≥ 1.5). The normalized abundance of SAG was included in the network analysis. The adjacency matrix was calculated using a power of 10 that satisfied the scale-free topology criterion. The dynamic tree cut method was used to define coregulation modules from the hierarchical tree based on topological overlap matrix, with the minimum module size set to 80 genes and the minimum height for merging modules set to 0.1. The eigengene value (first principal component) was calculated for each module and used to test the association with metabolite data. Subnetworks were similarly constructed by dividing the data into wild-type-like (wild-type, I6, and N31) and high SA (F10 and F52) groups, using a power of 14 for the adjacency matrix calculation. The networks were visualized using Cytoscape, with node colors corresponding to module colors from WGCNA. Selected genes were verified by qRT-PCR according to established protocols (Tsai et al., 2006) using elongation factor 1β, actin-related protein, and TATA box binding protein associated factor as housekeeping genes (see Supplemental Table 5 online for primers).

Meta-Analysis of *Populus* Leaf Microarray Data Sets

Populus leaf microarray data sets derived from oxidative stress experiments were downloaded from the Gene Expression Omnibus (GEO) and included Affymetrix (GSE9673, GSE15242, GSE16783, GSE16785, GSE17226, GSE17230, GSE21171, GSE27693, and GSE37608) and EST (GSE10873) microarray data. Affymetrix data were processed by MAS 5 (Affymetrix) and grouped in pairs containing stressed samples and their respective controls. The EST array data were normalized by print-tip LOWESS and quantile methods using codes provided by the original authors in GEO (Street et al., 2011). Quality control filtering was performed to remove probes (probe sets) that were below detection in each pair of samples (n = 2 to 3). DE was assessed by Limma using linear models (Smyth, 2005), and fold change of each probe (treatment/control) was calculated for all sample pairs. Probe annotation against *Populus* genome v2.2 was performed using an in-house pipeline and is available at http://aspendb.uga.edu/downloads. The fold change values and DE significance (P values) were then extracted for the 144 driver or 438 hub genes to generate box-and-whisker plots using *R* function box plot. Not all pairs contain all driver or hub genes due to quality control filtering, and the list of microarray sample pairs and their corresponding gene numbers are provided in Supplemental Table 4 online.

Accession Numbers

This Agilent microarray platform can be found in the National Center for Biotechnology Information GEO under accession number GPL16322 and is also available on the Agilent eArray website under "Published Designs" (ID 033484). The microarray data from this study can be found in GEO under accession number GSE42511. Expression values and annotation for the subset of genes used in network construction are provided in Supplemental Data Set 2 online. Accession numbers or gene model names for the other genes used in this work can be found in Supplemental Tables 3 and 5 online.

Supplemental Data

The following materials are available in the online version of this article.

Supplemental Figure 1. Screening Analysis of Independent Transgenic Lines.

Supplemental Figure 2. Electrolyte Leakage Analysis.

Supplemental Figure 3. Regression Analysis between Total SA and Total PGs, Total Chlorogenic Acids, or Individual Chlorogenic Acid Isomers.

Supplemental Figure 4. Gene Expression Changes in Response to Transgenic Manipulation.

Supplemental Figure 5. GO Enrichment Analysis of Differentially Expressed Genes.

Supplemental Figure 6. Properties of the Weighted Gene Correlation Network.

Supplemental Figure 7. Comparisons between the Wild-Type and FD-Irp9 Subnetworks.

Supplemental Figure 8. qRT-PCR Analysis of Representative *WRKY* and *RLK* Genes Identified by Microarray Analysis to Exhibit SA-Dependent Expression.

Supplemental Figure 9. Expression Responsiveness of the Hub Genes to Oxidative Stress Treatments Based on Meta-Analysis of Published *Populus* Leaf Microarray Data.

Supplemental Table 1. Repeated Measures ANOVA of Photosynthetic Responses Presented in Figure 2.

Supplemental Table 2. GO Enrichment of Network Module Members.

Supplemental Table 3. List of *NRX1* Probes, Their Gene Model Matches, and Sequence Identity Matrix.

Supplemental Table 4. List of Microarray Comparisons Used in the Meta-Analysis.

Supplemental Table 5. Primers Used in This Study.

Supplemental Data Set 1. Relative Abundance of Metabolites Identified by GC-MS or LC-TOF/MS.

Supplemental Data Set 2. List of Probes, Their Expression Values, and Network Module Assignment.

ACKNOWLEDGMENTS

We thank Jürgen Heesemann (Max von Pettenkofer-Institut, Munich, Germany) for providing the pTIrp9 plasmid, Syngenta Biotechnology for the *NahG* construct, Richard Lindroth (University of Wisconsin–Madison) for PG standards, Vanessa Michelizzi, Kate Tay, and Ousman Mahmud (University of Georgia) for technical assistance, and Stephen Pettis (University of Georgia) for greenhouse plant care. This work was funded by the U.S. National Science Foundation Grants DBI-0421756 and 0836433, the Georgia Research Alliance, and the Warnell School's Hank Haynes Forest Biotechnology endowment fund.

AUTHOR CONTRIBUTIONS

C.-J.T., S.A.H., and Y.Y. conceived the project and designed the experiments. Y.Y. designed and prepared the constructs. E.O.A. generated transgenic plants. W.G. performed all experiments and analyzed data. B.N., M.C.W., H.-Y.C., B.A.B., S.A.H., and C.-J.T. contributed to metabolite analyses. C.J.F. and S.A.H. performed photosynthesis analysis. L.-J.X. designed the microarray and performed all bioinformatics analyses. C.-J.T., L.-J.X., and S.A.H. wrote the article.

Received April 22, 2013; revised June 24, 2013; accepted July 10, 2013; published July 31, 2013.

REFERENCES

Afendi, F.M., Okada, T., Yamazaki, M., Hirai-Morita, A., Nakamura, Y., Nakamura, K., Ikeda, S., Takahashi, H., Altaf-Ul-Amin, M., Darusman, L.K., Saito, K., and Kanaya, S. (2012). KNApSAcK family databases: Integrated metabolite-plant species databases for multifaceted plant research. Plant Cell Physiol. **53:** e1.

Afzal, A.J., Wood, A.J., and Lightfoot, D.A. (2008). Plant receptor-like serine threonine kinases: Roles in signaling and plant defense. Mol. Plant Microbe Interact. **21:** 507–517.

Alexa, A., Rahnenführer, J., and Lengauer, T. (2006). Improved scoring of functional groups from gene expression data by decorrelating GO graph structure. Bioinformatics **22:** 1600–1607.

Allakhverdiev, S.I., Kreslavski, V.D., Klimov, V.V., Los, D.A., Carpentier, R., and Mohanty, P. (2008). Heat stress: An overview of molecular responses in photosynthesis. Photosynth. Res. **98:** 541–550.

Asada, K. (2006). Production and scavenging of reactive oxygen species in chloroplasts and their functions. Plant Physiol. **141:** 391–396.

Azaiez, A., Boyle, B., Levée, V., and Séguin, A. (2009). Transcriptome profiling in hybrid poplar following interactions with *Melampsora* rust fungi. Mol. Plant Microbe Interact. **22:** 190–200.

Babst, B.A., Harding, S.A., and Tsai, C.-J. (2010). Biosynthesis of phenolic glycosides from phenylpropanoid and benzenoid precursors in *Populus*. J. Chem. Ecol. **36:** 286–297.

Babushok, V.I., Linstrom, P.J., Reed, J.J., Zenkevich, I.G., Brown, R.L., Mallard, W.G., and Stein, S.E. (2007). Development of a database of gas chromatographic retention properties of organic compounds. J. Chromatogr. A **1157:** 414–421.

Barabási, A.-L., and Albert, R. (1999). Emergence of scaling in random networks. Science **286:** 509–512.

Basso, K., Margolin, A.A., Stolovitzky, G., Klein, U., Dalla-Favera, R., and Califano, A. (2005). Reverse engineering of regulatory networks in human B cells. Nat. Genet. **37:** 382–390.

Boeckler, G.A., Gershenzon, J., and Unsicker, S.B. (2011). Phenolic glycosides of the Salicaceae and their role as anti-herbivore defenses. Phytochemistry **72:** 1497–1509.

Caldana, C., Degenkolbe, T., Cuadros-Inostroza, A., Klie, S., Sulpice, R., Leisse, A., Steinhauser, D., Fernie, A.R., Willmitzer, L., and Hannah, M.A. (2011). High-density kinetic analysis of the metabolomic and transcriptomic response of *Arabidopsis* to eight environmental conditions. Plant J. **67:** 869–884.

Cao, H., Glazebrook, J., Clarke, J.D., Volko, S., and Dong, X. (1997). The *Arabidopsis* NPR1 gene that controls systemic acquired resistance encodes a novel protein containing ankyrin repeats. Cell **88:** 57–63.

Carter, C.J., and Thornburg, R.W. (2004). Tobacco nectarin V is a flavin-containing berberine bridge enzyme-like protein with glucose oxidase activity. Plant Physiol. **134:** 460–469.

Carter, S.L., Brechbühler, C.M., Griffin, M., and Bond, A.T. (2004). Gene co-expression network topology provides a framework for molecular characterization of cellular state. Bioinformatics **20:** 2242–2250.

Chen, J., Song, Y., Zhang, H., and Zhang, D. (2013). Genome-wide analysis of gene expression in response to drought stress in *Populus simonii.* Plant Mol. Biol. Rep. **31:** 946–962.

Chibani, K., Wingsle, G., Jacquot, J.-P., Gelhaye, E., and Rouhier, N. (2009). Comparative genomic study of the thioredoxin family in photosynthetic organisms with emphasis on *Populus trichocarpa*. Mol. Plant **2:** 308–322.

Clarke, S.M., Mur, L.A.J., Wood, J.E., and Scott, I.M. (2004). Salicylic acid dependent signaling promotes basal thermotolerance but is not essential for acquired thermotolerance in *Arabidopsis thaliana*. Plant J. **38:** 432–447.

Cohen, D., Bogeat-Triboulot, M.-B., Tisserant, E., Balzergue, S., Martin-Magniette, M.-L., Lelandais, G., Ningre, N., Renou, J.-P., Tamby, J.-P., Le Thiec, D., and Hummel, I. (2010). Comparative transcriptomics of drought responses in *Populus*: A meta-analysis of genome-wide expression profiling in mature leaves and root apices across two genotypes. BMC Genomics **11:** 630.

Custers, J.H.H.V., Harrison, S.J., Sela-Buurlage, M.B., van Deventer, E., Lageweg, W., Howe, P.W., van der Meijs, P.J., Ponstein, A.S., Simons, B.H., Melchers, L.S., and Stuiver, M.H. (2004). Isolation and characterisation of a class of carbohydrate oxidases from higher plants, with a role in active defence. Plant J. **39:** 147–160.

Czernic, P., Visser, B., Sun, W.N., Savouré, A., Deslandes, L., Marco, Y., Van Montagu, M., and Verbruggen, N. (1999). Characterization of an *Arabidopsis thaliana* receptor-like protein kinase gene activated by oxidative stress and pathogen attack. Plant J. **18:** 321–327.

Delaney, T.P., Uknes, S., Vernooij, B., Friedrich, L., Weymann, K., Negrotto, D., Gaffney, T., Gut-Rella, M., Kessmann, H., Ward, E., and Ryals, J. (1994). A central role of salicylic acid in plant disease resistance. Science **266:** 1247–1250.

Diara, C., Castagna, A., Baldan, B., Sodi, A.M., Sahr, T., Langebartels, C., Sebastiani, L., and Ranieri, A. (2005). Differences in the kinetics and scale of signalling molecule production modulate the ozone sensitivity of hybrid poplar clones: Tthe roles of H_2O_2, ethylene and salicylic acid. New Phytol. **168:** 351–364.

Dong, X.N. (2001). Genetic dissection of systemic acquired resistance. Curr. Opin. Plant Biol. **4:** 309–314.

Du, Z., Zhou, X., Ling, Y., Zhang, Z., and Su, Z. (2010). agriGO: A GO analysis toolkit for the agricultural community. Nucleic Acids Res. **38** (Web Server issue)**:** W64–W70.

Foyer, C.H., and Noctor, G. (2005). Redox homeostasis and antioxidant signaling: A metabolic interface between stress perception and physiological responses. Plant Cell **17:** 1866–1875.

Frost, C.J., Nyamdari, B., Tsai, C.-J., and Harding, S.A. (2012). The tonoplast-localized sucrose transporter in *Populus* (PtaSUT4) regulates whole-plant water relations, responses to water stress, and photosynthesis. PLoS ONE **7:** e44467.

Gaffney, T., Friedrich, L., Vernooij, B., Negrotto, D., Nye, G., Uknes, S., Ward, E., Kessmann, H., and Ryals, J. (1993). Requirement of salicylic acid for the induction of systemic acquired resistance. Science **261:** 754–756.

Garcion, C., Lohmann, A., Lamodière, E., Catinot, J., Buchala, A., Doermann, P., and Métraux, J.-P. (2008). Characterization and biological function of the ISOCHORISMATE SYNTHASE2 gene of *Arabidopsis*. Plant Physiol. **147:** 1279–1287.

Germain, H., and Séguin, A. (2011). Innate immunity: Has poplar made its BED? New Phytol. **189:** 678–687.

Hamanishi, E.T., Raj, S., Wilkins, O., Thomas, B.R., Mansfield, S.D., Plant, A.L., and Campbell, M.M. (2010). Intraspecific variation in the *Populus balsamifera* drought transcriptome. Plant Cell Environ. **33:** 1742–1755.

Hennig, J., Malamy, J., Grynkiewicz, G., Indulski, J., and Klessig, D.F. (1993). Interconversion of the salicylic acid signal and its glucoside in tobacco. Plant J. **4:** 593–600.

Hozain, M.I., Salvucci, M.E., Fokar, M., and Holaday, A.S. (2010). The differential response of photosynthesis to high temperature for a boreal and temperate *Populus* species relates to differences in Rubisco activation and Rubisco activase properties. Tree Physiol. **30:** 32–44.

Jeong, H., Mason, S.P., Barabási, A.L., and Oltvai, Z.N. (2001). Lethality and centrality in protein networks. Nature **411:** 41–42.

Jeong, M.L., Jiang, H.Y., Chen, H.S., Tsai, C.J., and Harding, S.A. (2004). Metabolic profiling of the sink-to-source transition in developing leaves of quaking aspen. Plant Physiol. **136:** 3364–3375.

Joët, T., Salmona, J., Laffargue, A., Descroix, F., and Dussert, S. (2010). Use of the growing environment as a source of variation to identify the quantitative trait transcripts and modules of co-expressed genes that determine chlorogenic acid accumulation. Plant Cell Environ. **33:** 1220–1233.

Jung, H.W., Tschaplinski, T.J., Wang, L., Glazebrook, J., and Greenberg, J.T. (2009). Priming in systemic plant immunity. Science **324:** 89–91.

Kaplan, F., Kopka, J., Haskell, D.W., Zhao, W., Schiller, K.C., Gatzke, N., Sung, D.Y., and Guy, C.L. (2004). Exploring the temperature-stress metabolome of *Arabidopsis*. Plant Physiol. **136:** 4159–4168.

Kawano, T., Tanaka, S., Kadono, T., and Muto, S. (2004). Salicylic acid glucoside acts as a slow inducer of oxidative burst in tobacco suspension culture. Z. Naturforsch. C . **59:** 684–692.

Khokon, A.R., Okuma, E., Hossain, M.A., Munemasa, S., Uraji, M., Nakamura, Y., Mori, I.C., and Murata, Y. (2011). Involvement of extracellular oxidative burst in salicylic acid-induced stomatal closure in *Arabidopsis*. Plant Cell Environ. **34:** 434–443.

Kind, T., Wohlgemuth, G., Lee, Y., Lu, Y., Palazoglu, M., Shahbaz, S., and Fiehn, O. (2009). FiehnLib: Mass spectral and retention index libraries for metabolomics based on quadrupole and time-of-flight gas chromatography/mass spectrometry. Anal. Chem. **81:** 10038–10048.

Koch, J.R., Creelman, R.A., Eshita, S.M., Seskar, M., Mullet, J.E., and Davis, K.R. (2000). Ozone sensitivity in hybrid poplar correlates with insensitivity to both salicylic acid and jasmonic acid. The role of programmed cell death in lesion formation. Plant Physiol. **123:** 487–496.

Kovtun, Y., Chiu, W.-L., Tena, G., and Sheen, J. (2000). Functional analysis of oxidative stress-activated mitogen-activated protein kinase cascade in plants. Proc. Natl. Acad. Sci. USA **97:** 2940–2945.

Langfelder, P., and Horvath, S. (2008). WGCNA: An *R* package for weighted correlation network analysis. BMC Bioinformatics **9:** 559.

Larkindale, J., and Knight, M.R. (2002). Protection against heat stress-induced oxidative damage in *Arabidopsis* involves calcium, abscisic acid, ethylene, and salicylic acid. Plant Physiol. **128:** 682–695.

Lee, J.-S. (1998). The mechanism of stomatal closing by salicylic acid in *Commelina communis* L. J. Plant Biol. **41:** 97–102.

Lee, S., Choi, H., Suh, S., Doo, I.-S., Oh, K.-Y., Choi, E.J., Schroeder Taylor, A.T., Low, P.S., and Lee, Y. (1999). Oligogalacturonic acid and chitosan reduce stomatal aperture by inducing the evolution of reactive oxygen species from guard cells of tomato and *Commelina communis*. Plant Physiol. **121:** 147–152.

Lehti-Shiu, M.D., and Shiu, S.-H. (2012). Diversity, classification and function of the plant protein kinase superfamily. Philos. Trans. R. Soc. Lond. B Biol. Sci. **367:** 2619–2639.

Lehti-Shiu, M.D., Zou, C., Hanada, K., and Shiu, S.-H. (2009). Evolutionary history and stress regulation of plant receptor-like kinase/pelle genes. Plant Physiol. **150:** 12–26.

Loake, G., and Grant, M. (2007). Salicylic acid in plant defence—The players and protagonists. Curr. Opin. Plant Biol. **10:** 466–472.

Mahdi, J.G., Mahdi, A.J., Mahdi, A.J., and Bowen, I.D. (2006). The historical analysis of aspirin discovery, its relation to the willow tree and antiproliferative and anticancer potential. Cell Prolif. **39:** 147–155.

Mateo, A., Funck, D., Mühlenbock, P., Kular, B., Mullineaux, P.M., and Karpinski, S. (2006). Controlled levels of salicylic acid are required for optimal photosynthesis and redox homeostasis. J. Exp. Bot. **57:** 1795–1807.

Meilan, R., and Ma, C. (2006). Poplar (*Populus* spp.). In Methods in Molecular Biology: Agrobacterium Protocols, Vol. 34, K. Wang, ed (Totowa, NJ: Humana Press), pp. 143–151.

Melotto, M., Underwood, W., Koczan, J., Nomura, K., and He, S.Y. (2006). Plant stomata function in innate immunity against bacterial invasion. Cell **126:** 969–980.

Mondolot, L., La Fisca, P., Buatois, B., Talansier, E., de Kochko, A., and Campa, C. (2006). Evolution in caffeoylquinic acid content and histolocalization during *Coffea canephora* leaf development. Ann. Bot. (Lond.) **98:** 33–40.

Mori, I.C., Pinontoan, R., Kawano, T., and Muto, S. (2001). Involvement of superoxide generation in salicylic acid-induced stomatal closure in *Vicia faba*. Plant Cell Physiol. **42:** 1383–1388.

Morris, E.R., and Walker, J.C. (2003). Receptor-like protein kinases: The keys to response. Curr. Opin. Plant Biol. **6:** 339–342.

Morse, A.M., Tschaplinski, T.J., Dervinis, C., Pijut, P.M., Schmelz, E.A., Day, W., and Davis, J.M. (2007). Salicylate and catechol levels are maintained in nahG transgenic poplar. Phytochemistry **68:** 2043–2052.

Nakatani, N., Kayano, S.-i., Kikuzaki, H., Sumino, K., Katagiri, K., and Mitani, T. (2000). Identification, quantitative determination, and antioxidative activities of chlorogenic acid isomers in prune (*Prunus domestica* L.). J. Agric. Food Chem. **48:** 5512–5516.

Nawrath, C., and Métraux, J.-P. (1999). Salicylic acid induction-deficient mutants of *Arabidopsis* express PR-2 and PR-5 and accumulate high levels of camalexin after pathogen inoculation. Plant Cell **11:** 1393–1404.

Niggeweg, R., Michael, A.J., and Martin, C. (2004). Engineering plants with increased levels of the antioxidant chlorogenic acid. Nat. Biotechnol. **22:** 746–754.

Nogués, S., Allen, D.J., Morison, J.I.L., and Baker, N.R. (1999). Characterization of stomatal closure caused by ultraviolet-B radiation. Plant Physiol. **121:** 489–496.

Ohtake, Y., Takahashi, T., and Komeda, Y. (2000). Salicylic acid induces the expression of a number of receptor-like kinase genes in *Arabidopsis thaliana*. Plant Cell Physiol. **41:** 1038–1044.

Payyavula, R.S., Babst, B.A., Nelsen, M.P., Harding, S.A., and Tsai, C.-J. (2009). Glycosylation-mediated phenylpropanoid partitioning in *Populus tremuloides* cell cultures. BMC Plant Biol. **9:** 151.

Pelludat, C., Brem, D., and Heesemann, J. (2003). Irp9, encoded by the high-pathogenicity island of *Yersinia enterocolitica*, is able to convert chorismate into salicylate, the precursor of the siderophore yersiniabactin. J. Bacteriol. **185:** 5648–5653.

Pierpoint, W.S. (1994). Salicylic acid and its derivatives in plants: Medicines, metabolites and messenger molecules. Adv. Bot. Res. **20:** 163–235.

Poór, P., Gémes, K., Horváth, F., Szepesi, A., Simon, M.L., and Tari, I. (2011). Salicylic acid treatment via the rooting medium interferes with stomatal response, CO_2 fixation rate and carbohydrate metabolism in tomato, and decreases harmful effects of subsequent salt stress. Plant Biol. (Stuttg.) **13:** 105–114.

Raj, S., Bräutigam, K., Hamanishi, E.T., Wilkins, O., Thomas, B.R., Schroeder, W., Mansfield, S.D., Plant, A.L., and Campbell, M.M. (2011). Clone history shapes *Populus* drought responses. Proc. Natl. Acad. Sci. USA **108:** 12521–12526.

Ramachandran, S., Fontanille, P., Pandey, A., and Larroche, C. (2006). Gluconic acid: Properties, applications and microbial production. Food Technol. Biotechnol. **44:** 185–195.

Rao, M.V., and Davis, K.R. (1999). Ozone-induced cell death occurs via two distinct mechanisms in *Arabidopsis*: The role of salicylic acid. Plant J. **17:** 603–614.

Raskin, I. (1992). Role of salicylic acid in plants. Annu. Rev. Plant Physiol. Plant Mol. Biol. **43:** 439–463.

Rivas-San Vicente, M., and Plasencia, J. (2011). Salicylic acid beyond defence: Its role in plant growth and development. J. Exp. Bot. **62:** 3321–3338.

Scherer, G.F.E., Ryu, S.B., Wang, X., Matos, A.R., and Heitz, T. (2010). Patatin-related phospholipase A: Nomenclature, subfamilies and functions in plants. Trends Plant Sci. **15:** 693–700.

Sharma, Y.K., Léon, J., Raskin, I., and Davis, K.R. (1996). Ozone-induced responses in *Arabidopsis thaliana*: The role of salicylic acid in the accumulation of defense-related transcripts and induced resistance. Proc. Natl. Acad. Sci. USA **93:** 5099–5104.

Smoot, M.E., Ono, K., Ruscheinski, J., Wang, P.-L., and Ideker, T. (2011). Cytoscape 2.8: New features for data integration and network visualization. Bioinformatics **27:** 431–432.

Smyth, G.K. (2005). Limma: Linear models for microarray data. In Bioinformatics and Computational Biology Solutions Using R and Bioconductor, R. Gentleman, V. Carey, S. Dudoit, R. Irizarry, and W. Huber, eds (New York: Springer), pp. 397–420.

Street, N.R., James, T.M., James, T., Mikael, B., Jaakko, K., Mark, B., and Taylor, G. (2011). The physiological, transcriptional and genetic responses of an ozone-sensitive and an ozone tolerant poplar and selected extremes of their F2 progeny. Environ. Pollut. **159:** 45–54.

Syed, H.A., and Threadgill, D.W. (2006). Enhanced oligonucleotide microarray labeling and hybridization. Biotechniques **41:** 685–686.

Tada, Y., Spoel, S.H., Pajerowska-Mukhtar, K., Mou, Z., Song, J., Wang, C., Zuo, J., and Dong, X. (2008). Plant immunity requires conformational changes [corrected] of NPR1 via S-nitrosylation and thioredoxins. Science **321:** 952–956.

Terpstra, I.R., Snoek, L.B., Keurentjes, J.J.B., Peeters, A.J.M., and van den Ackerveken, G. (2010). Regulatory network identification by genetical genomics: signaling downstream of the *Arabidopsis* receptor-like kinase ERECTA. Plant Physiol. **154:** 1067–1078.

Tsai, C.J., Cseke, L.J., and Harding, S.A. (2011a). Isolation and purification of RNA. In Handbook of Molecular and Cellular Methods in Biology and Medicine, L.J. Cseke, A. Kirakosyan, P.B. Kaufman, and M.V. Westfall, eds (Boca Raton, FL: CRC Press), pp. 167–186.

Tsai, C.J., Harding, S.A., Tschaplinski, T.J., Lindroth, R.L., and Yuan, Y. (2006). Genome-wide analysis of the structural genes regulating defense phenylpropanoid metabolism in *Populus*. New Phytol. **172:** 47–62.

Tsai, C.J., Ranjan, P., DiFazio, S.P., Tuskan, G.A., and Johnson, V. (2011b). Poplar genome microarrays. In Genetics, Genomics and Breeding of Poplars, C.P. Joshi, S.P. DiFazio, and C. Kole, eds (Enfield, NH: Science Publishers), pp. 112–127.

Vahala, J., Keinänen, M., Schützendübel, A., Polle, A., and Kangasjärvi, J. (2003). Differential effects of elevated ozone on two hybrid aspen genotypes predisposed to chronic ozone fumigation. Role of ethylene and salicylic acid. Plant Physiol. **132:** 196–205.

Verberne, M.C., Verpoorte, R., Bol, J.F., Mercado-Blanco, J., and Linthorst, H.J.M. (2000). Overproduction of salicylic acid in plants by bacterial transgenes enhances pathogen resistance. Nat. Biotechnol. **18:** 779–783.

Vlot, A.C., Dempsey, D.A., and Klessig, D.F. (2009). Salicylic acid, a multifaceted hormone to combat disease. Annu. Rev. Phytopathol. **47:** 177–206.

Wang, H.-Q., Tuominen, L.K., and Tsai, C.-J. (2011). SLIM: A sliding linear model for estimating the proportion of true null hypotheses in datasets with dependence structures. Bioinformatics **27:** 225–231.

Wang, L., Wang, B.-L., Wei, Z.-Z., Du, Q.-Z., Zhang, D.-Q., and Li, B.-L. (2012). Development of 35 microsatellite markers from heat stress transcription factors in *Populus simonii* (Salicaceae). Am. J. Bot. **99:** e357–e361.

Weston, D.J., Karve, A.A., Gunter, L.E., Jawdy, S.S., Yang, X., Allen, S.M., and Wullschleger, S.D. (2011). Comparative physiology and transcriptional networks underlying the heat shock response in *Populus trichocarpa*, *Arabidopsis thaliana* and *Glycine max*. Plant Cell Environ. **34:** 1488–1506.

Wildermuth, M.C., Dewdney, J., Wu, G., and Ausubel, F.M. (2001). Isochorismate synthase is required to synthesize salicylic acid for plant defence. Nature **414:** 562–565.

Wilkins, O., Waldron, L., Nahal, H., Provart, N.J., and Campbell, M.M. (2009). Genotype and time of day shape the *Populus* drought response. Plant J. **60:** 703–715.

Wu, G., Shortt, B.J., Lawrence, E.B., Levine, E.B., Fitzsimmons, K.C., and Shah, D.M. (1995). Disease resistance conferred by expression of a gene encoding H_2O_2-generating glucose oxidase in transgenic potato plants. Plant Cell **7:** 1357–1368.

Wu, Y., Zhang, D., Chu, J.Y., Boyle, P., Wang, Y., Brindle, I.D., De Luca, V., and Després, C. (2012). The *Arabidopsis* NPR1 protein is a receptor for the plant defense hormone salicylic acid. Cell Rep. **1:** 639–647.

Xu, X., Chen, C., Fan, B., and Chen, Z. (2006). Physical and functional interactions between pathogen-induced *Arabidopsis* WRKY18, WRKY40, and WRKY60 transcription factors. Plant Cell **18:** 1310–1326.

Yalpani, N., Enyedi, A.J., León, J., and Raskin, I. (1994). Ultraviolet light and ozone stimulate accumulation of salicylic acid, pathogenesis-related proteins and virus resistance in tobacco. Planta **193:** 372–376.

Yu, G., Li, F., Qin, Y., Bo, X., Wu, Y., and Wang, S. (2010). GOSemSim: An R package for measuring semantic similarity among GO terms and gene products. Bioinformatics **26:** 976–978.

Yuan, Y., Chung, J.-D., Fu, X., Johnson, V.E., Ranjan, P., Booth, S. L., Harding, S.A., and Tsai, C.-J. (2009). Alternative splicing and gene duplication differentially shaped the regulation of isochorismate synthase in *Populus* and *Arabidopsis*. Proc. Natl. Acad. Sci. USA **106:** 22020–22025.

Zeng, W., Melotto, M., and He, S.Y. (2010). Plant stomata: A checkpoint of host immunity and pathogen virulence. Curr. Opin. Biotechnol. **21:** 599–603.

Zenk, M.H. (1967). Pathways of salicyl alcohol and salicin formation in *Salix purpurea* L. Phytochemistry **6:** 245–252.

Zoeller, M., Stingl, N., Krischke, M., Fekete, A., Waller, F., Berger, S., and Mueller, M.J. (2012). Lipid profiling of the *Arabidopsis* hypersensitive response reveals specific lipid peroxidation and fragmentation processes: Biogenesis of pimelic and azelaic acid. Plant Physiol. **160:** 365–378.

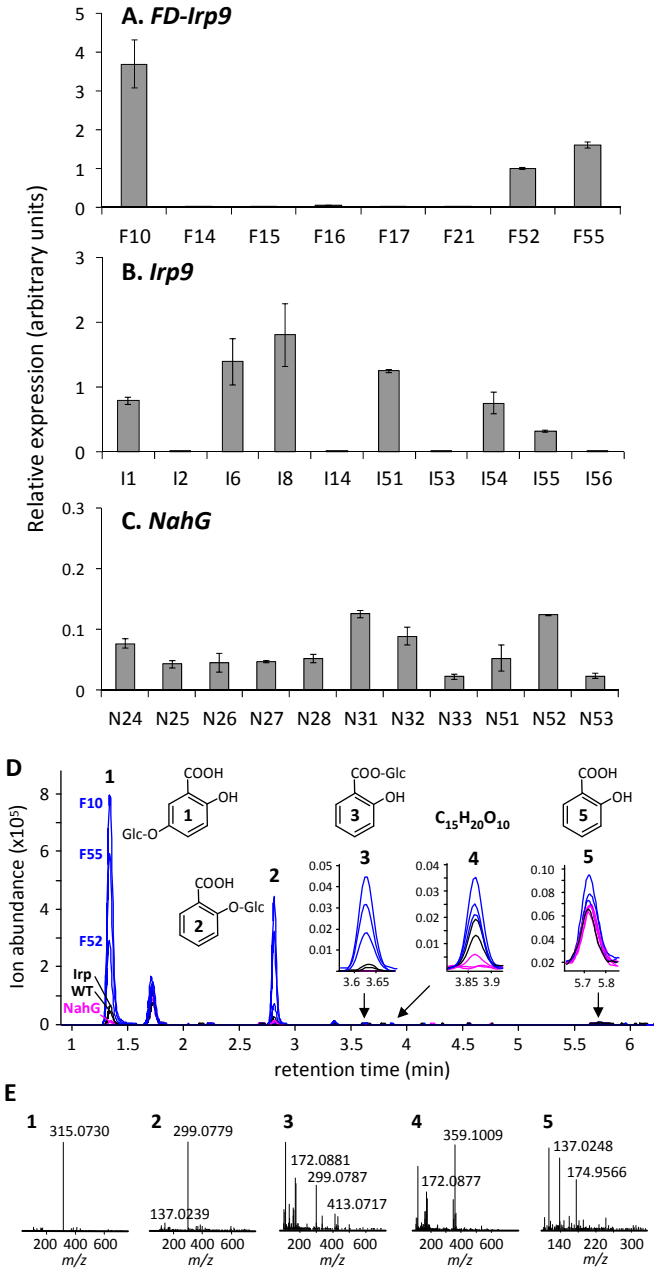

Supplemental Figure 1. Screening analysis of independent transgenic lines.
(A) to **(C)** qRT-PCR analysis of FD-Irp9 **(A)**, Irp9 **(B)** and NahG **(C)** transgenic lines. Bars are means ± SD of two technical replicates. Expression in WT was below detection. **(D)** to **(E)** Relative abundance of SA metabolites in representative transgenic and WT plants. Shown are extracted ion chromatograms **(D)** and mass spectral fragmentation patterns **(E)** of gentisic acid glucoside (1), SA glucoside (2), SA glucose ester (3), putative syringic acid glucoside (4), and SA (5). Blue and pink traces are FD-Irp9 and NahG lines, respectively, while WT and Irp9 are shown in black.

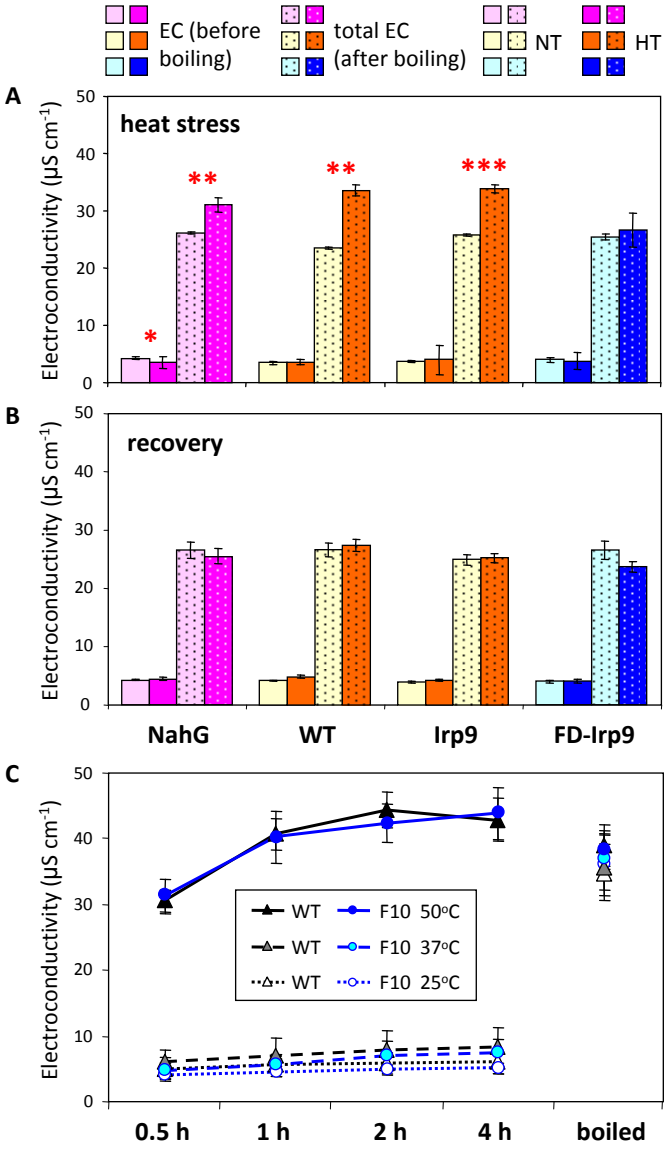

Supplemental Figure 2. Electrolyte leakage analysis.
(A) to **(B)** Leaf discs were sampled one week after heat treatment **(A)** or recovery **(B)** from the two-chamber heat experiment. Data represent means ± SE using pooled transgenic lines and/or biological replicates (n= 7-12). Statistical significance between normal (NT) and high temperature (HT) conditions was evaluated by the two-sample *t*-test (*** $p \leq 0.001$; ** $0.001 < p \leq 0.01$, * $0.01 < p \leq 0.05$).
(C) Leaf discs from greenhouse-grown WT and FD-Irp9 (F10) plants were incubated at 25°C, 37°C or 50°C for the indicated time prior to electroconductivity measurements (n= 5). Repeated measures ANOVA showed a significant temperature effect ($p \leq 0.001$) as expected, but the differences between genotypes were not significant ($p = 0.7$).

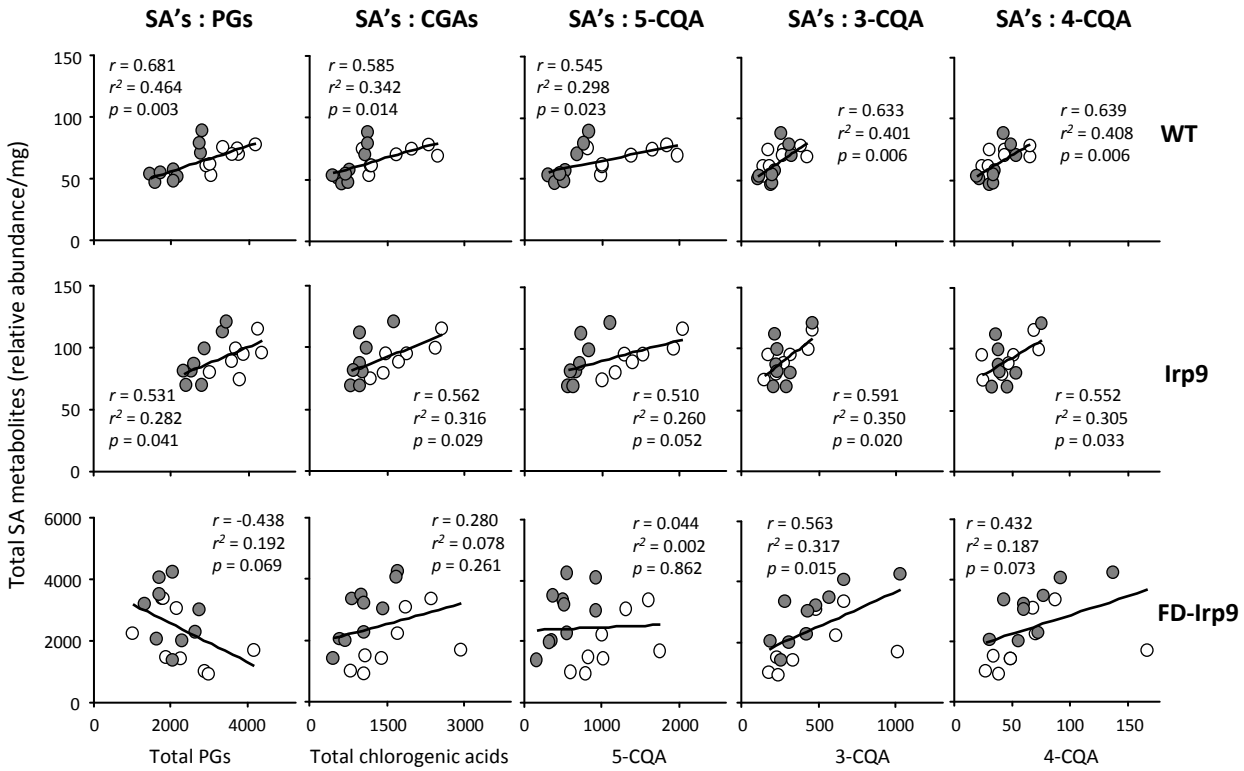

Supplemental Figure 3. Regression analysis between total SA and total PGs, total chlorogenic acids or individual chlorogenic acid isomers.

Data from all transgenic lines and/or biological replicates within each genotype were used for the analysis (n= 7-9). The NahG group was excluded from the analysis, as the total SA levels were relatively invariable. The total SA levels are represented as the sum of the normalized peak area of SA, SAG, SA glucose ester and gentisic acid glucoside; total PGs as the sum of salicin, salicortin and tremulacin; and total CGAs as the sum of 3-CQA, 4-CQA and 5-CQA. Open and filled symbols were from normal and high temperature conditions, respectively. CGA, chlorogenic acid; CQA, caffeoylquinic acid.

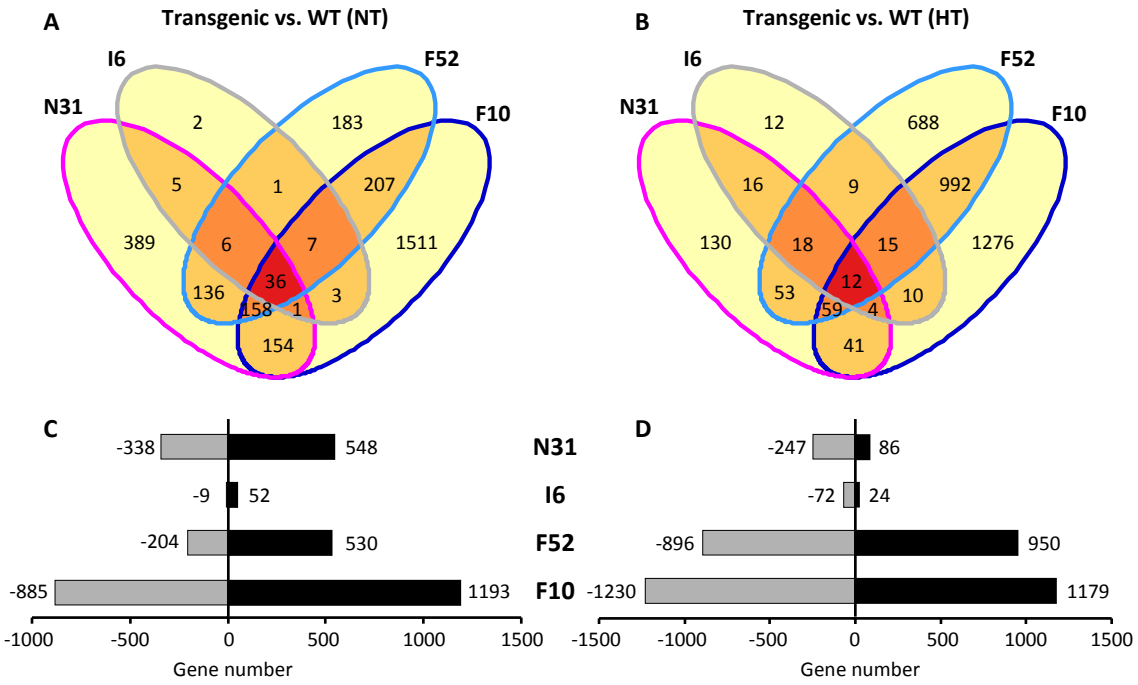

Supplemental Figure 4. Gene expression changes in response to transgenic manipulation.
(A) to **(B)** Venn diagrams of genes significantly changed in the transgenics relative to WT under normal **(A)** or high **(B)** temperatures.
(C) to **(D)** Breakdown of up-regulated (black bars, positive numbers) and down-regulated (grey bars, negative numbers) under normal **(C)** or high **(D)** temperatures.

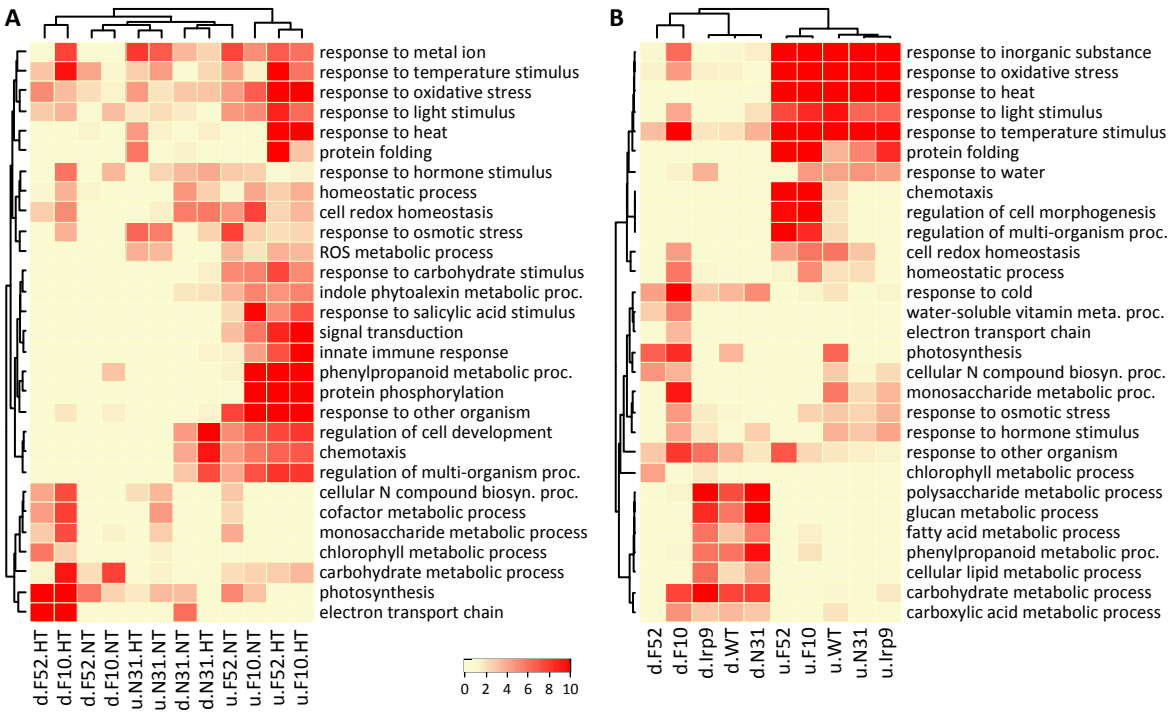

Supplemental Figure 5. GO enrichment analysis of differentially expressed genes.
(A) GO enrichment patterns of genes significantly affected by transgenic manipulation under normal (NT) or high temperature (HT) conditions.
(B) GO enrichment patterns of heat-responsive genes in WT and transgenic lines. Significantly enriched GO terms from up (u)- or down (d)-regulated genes of each genotype/treatment comparison were subjected to clustering analysis using the negative log10 transformed *p* values and visualized in heatmaps according to the color scale. Genotype/treatment comparisons are arranged in columns, while enrichment significance of GO terms is shown in rows.

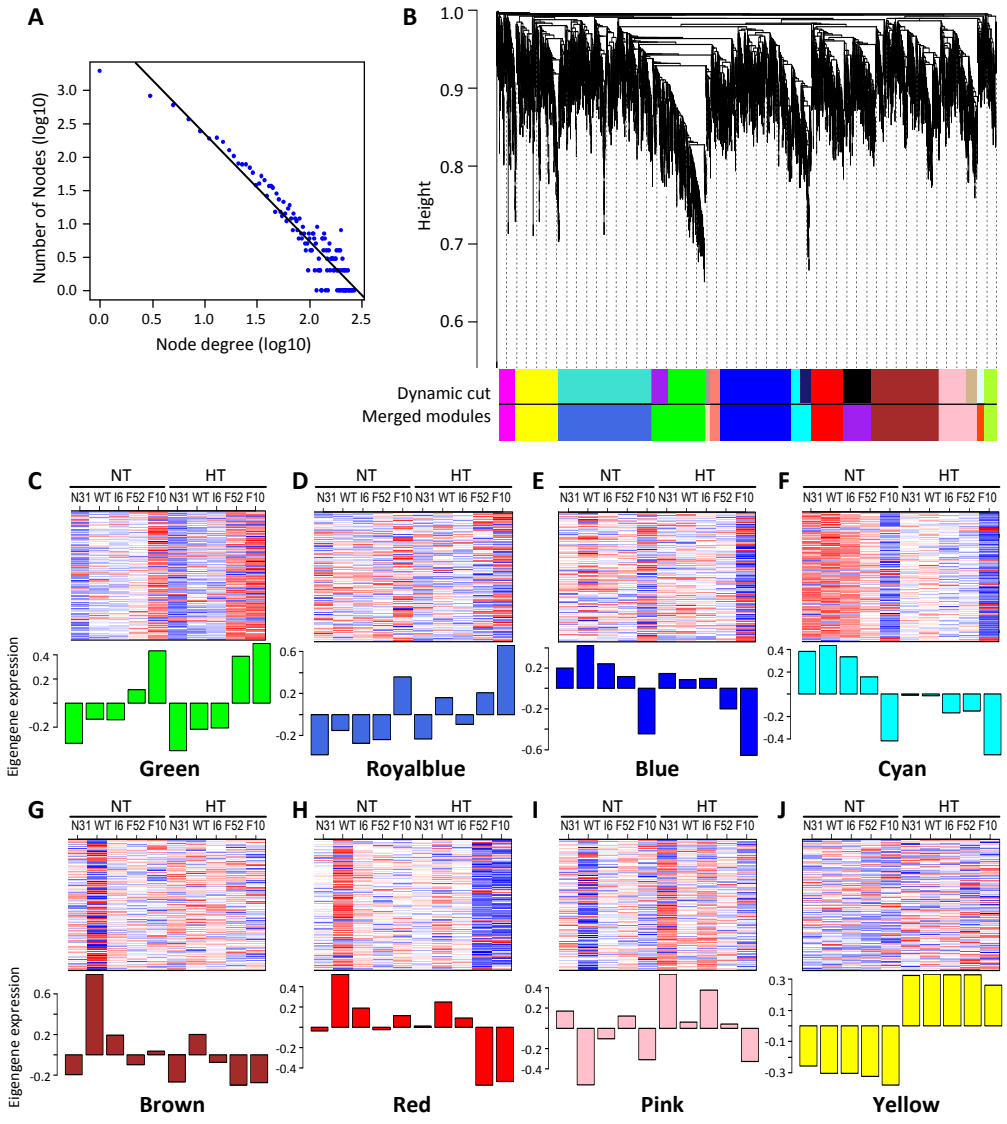

Supplemental Figure 6. Properties of the weighted gene correlation network.
(A) Distribution of the node degree of the reconstructed network follows a power-law behavior.
(B) Module assignment using the dynamic tree cut method.
(C) to **(J)** Expression profiles of module gene members and module eigengene are shown by heatmap (top) and bar graph (bottom), respectively, in each panel for representative modules.

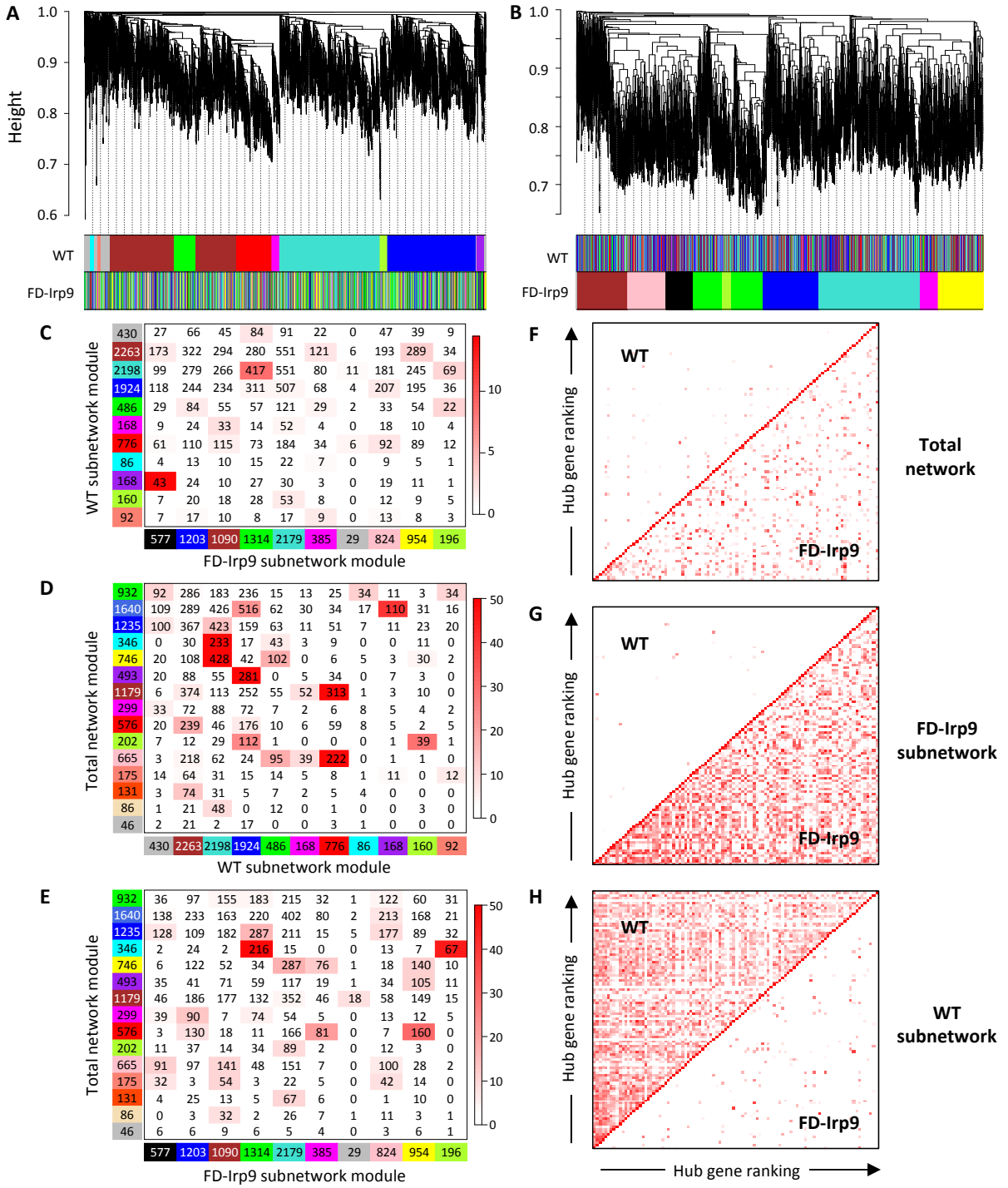

Supplemental Figure 7. Comparisons between the WT and FD-Irp9 subnetworks.

(A) to **(B)** Module assignment for the WT **(A)** and FD-Irp9 **(B)** subnetworks. Corresponding module assignment from the other subnetwork is also shown.

(C) to **(E)** Module similarity analysis between the two subnetworks **(C)**, or between the total network with the WT subnetwork **(D)** or the FD-Irp9 subnetwork **(E)**. Numbers of overlapping genes for all pairwise module analysis are shown.

(F) to **(H)** Heatmap plots of hub gene similarity among networks. The top 100 most highly connected hub genes from the total network **(F)** or the FD-Irp9 **(G)** or WT **(H)** subnetwork were obtained and their connectivity in the corresponding WT (upper half) or FD-Irp9 subnetwork (lower half) is shown. Arrows indicate decreasing hub gene ranking (connectivity) and color denotes the degree of connectivity (darker color = higher connectivity).

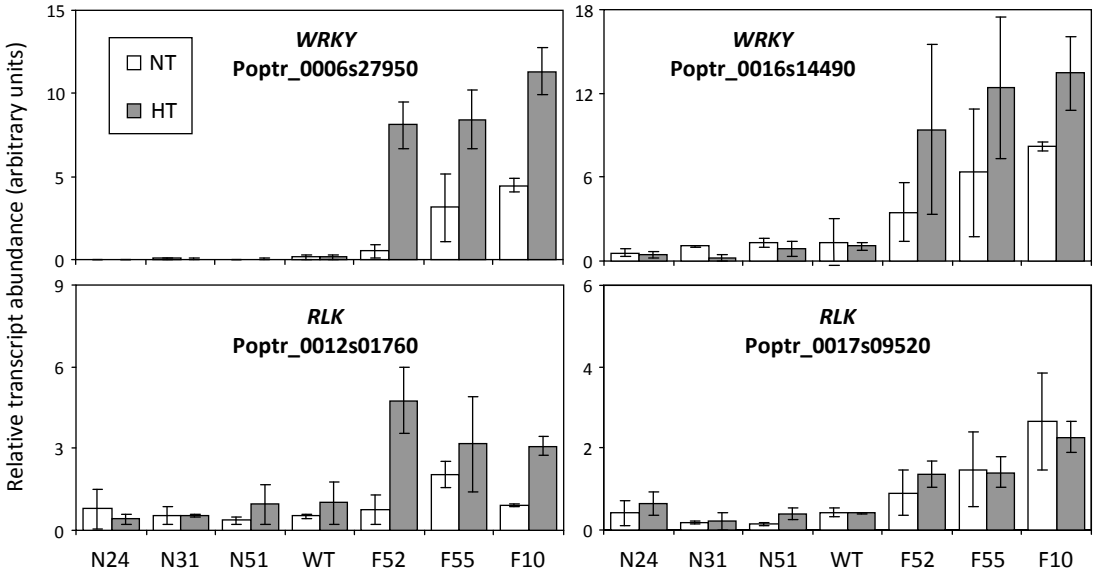

Supplemental Figure 8. qRT-PCR analysis of representative *WRKY* and *RLK* genes identified by microarray analysis to exhibit SA-dependent expression.

Data represent means ± SD of 2-3 biological replicates. NT, normal temperature; HT, high temperature.

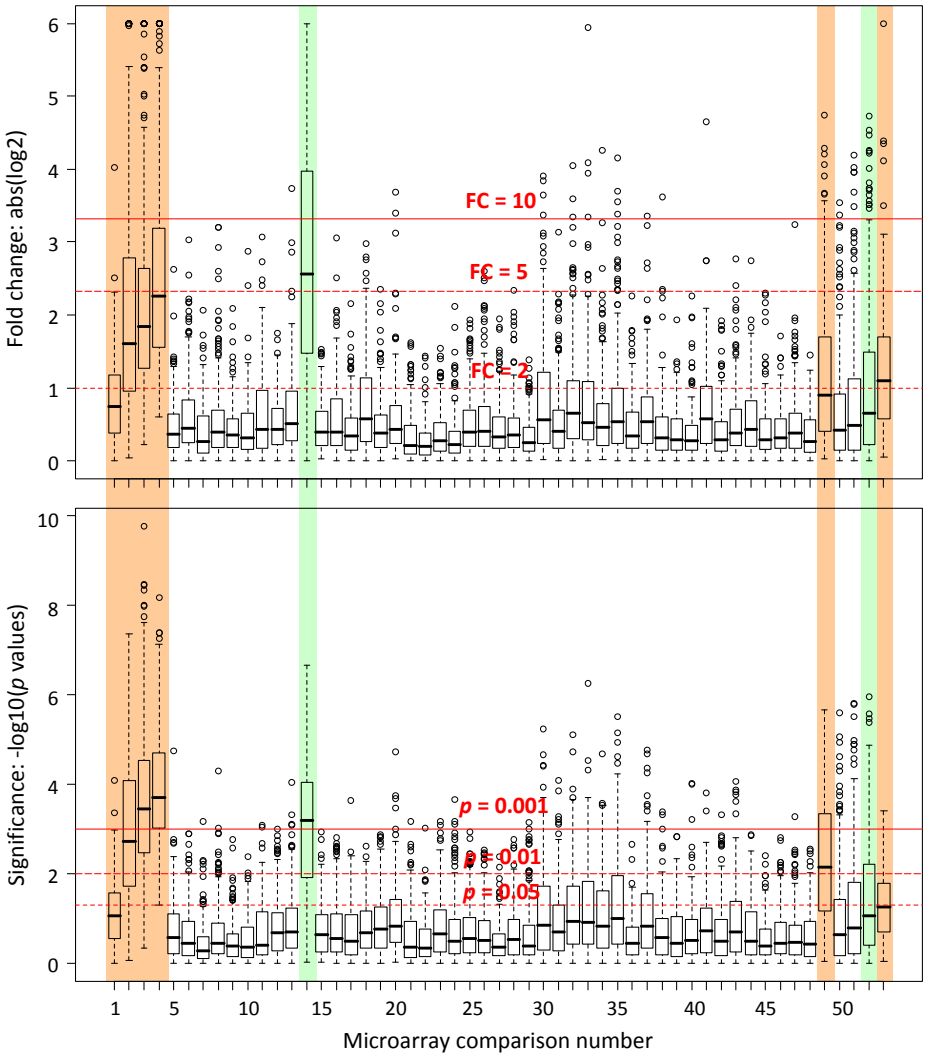

Supplemental Figure 9. Expression responsiveness of the hub genes to oxidative stress treatments based on meta-analysis of published *Populus* leaf microarray data.
Gene expression differences between stressed samples and their respective controls were assessed by fold-change (FC, top panel) or statistical significance (*p*-value, bottom panel). Horizontal red lines depict three arbitrary thresholds in each panel. Stress experiments are color-highlighted as in Figure 9, including SA and/or heat (nos. 1-4, this study), wounding (no. 14), drought (no. 49), pathogen infection (no. 52) and ozone (no. 53). Note the overall weaker responses of the hub genes compared to the driver genes shown in Figure 9. See Supplemental Table 4 for the complete list of comparisons and data source.

Supplemental Table 1. Repeated measures ANOVA of photosynthetic responses presented in Figure 2. Significant genotypic effects were further analyzed by pairwise comparison between WT and individual transgenic lines. Df(num), numerator degrees of freedom; Df(den), denominator degrees of freedom.

Leaf	Measurement	Source	*Df(num)*	*Df(den)*	*F*	*Pr > F*
LPI-10	Net photosyntehsis	genotype	4	24	2.983	0.0393
		treatment	4	96	11.813	<0.0001
		genotype x treatment	16	96	3.180	0.0002
		WT vs. F52	1	14	3.608	0.0783
		WT vs. F55	1	11	9.210	0.0114
		WT vs. N24	1	12	1.490	0.2456
		WT vs. N31	1	14	3.023	0.1040
	Conductance	genotype	4	24	11.137	<0.0001
		treatment	4	96	9.477	<0.0001
		genotype:treatment	16	96	1.614	0.0795
		WT vs. F52	1	14	20.373	0.0005
		WT vs. F55	1	11	24.351	0.0004
		WT vs. N24	1	12	2.402	0.1471
		WT vs. N31	1	14	0.044	0.8369
	Transpiration	genotype	4	24	14.905	<0.0001
		treatment	4	96	248.961	<0.0001
		genotype:treatment	16	96	3.711	<0.0001
		WT vs. F52	1	14	25.205	0.0002
		WT vs. F55	1	11	45.022	<0.0001
		WT vs. N24	1	12	1.513	0.2423
		WT vs. N31	1	14	0.094	0.7643
LPI-5	Net photosyntehsis	Genotype	4	24	1.464	0.2442
		Treatment	4	96	37.760	<.0001
		Genotype x treatment	16	96	0.604	0.8738
		WT vs. F52	1	14	2.625	0.1275
		WT vs. F55	1	11	2.927	0.1151
		WT vs. N24	1	12	1.202	0.2944
		WT vs. N31	1	14	3.594	0.0788
	Conductance	genotype	4	24	5.818	0.0020
		treatment	4	96	18.021	<0.0001
		genotype:treatment	16	96	1.453	0.1343
		WT vs. F52	1	14	1.300	0.2734
		WT vs. F55	1	11	2.714	0.1277
		WT vs. N24	1	12	19.106	0.0009
		WT vs. N31	1	14	4.537	0.0514
	Transpiration	genotype	4	24	3.217	0.0300
		treatment	4	96	552.006	<0.0001
		genotype:treatment	16	96	1.131	0.3386
		WT vs. F52	1	14	1.444	0.2494
		WT vs. F55	1	11	2.305	0.1571
		WT vs. N24	1	12	8.721	0.0121
		WT vs. N31	1	14	2.861	0.1129

Supplemental Table 2. GO enrichment of network module members.

GO	Term	No. in genome	Royal blue (I)	Green (II)	Blue (V)	Cyan (VI)	Brown (VII)	Red (IX)	Yellow (XII)	Pink (XIII)
GO:0048589	developmental growth	471	0.4	2.4	0.1	3.6	1.6	0.1	0.1	0.6
GO:0060560	developmental growth involved in morphogensis	394	0.5	3.0	0.1	3.7	1.8	0.1	0.2	0.9
GO:0006950	response to stress	4778	3.1	5.8	0.5	0.0	1.3	2.6	10.0	1.6
GO:0006952	defense response	2073	1.1	12.7	0.0	0.0	0.0	0.3	0.0	0.0
GO:0050832	defense response to fungus	392	1.8	12.9	1.0	0.3	0.0	0.0	0.1	0.0
GO:0006970	response to osmotic stress	902	3.8	0.7	1.6	0.4	1.0	1.0	3.7	2.6
GO:0006979	response to oxidative stress	588	1.7	4.2	0.3	0.1	1.1	3.8	12.9	0.9
GO:0000302	response to reactive oxygen species	150	2.5	0.1	0.0	0.0	0.0	1.6	9.4	1.9
GO:0042542	response to hydrogen peroxide	100	1.3	0.1	0.0	0.0	0.0	0.1	11.3	1.0
GO:0009408	response to heat	288	1.9	0.0	0.4	0.2	0.0	0.1	30.0	1.0
GO:0042221	response to chemical stimulus	4125	1.0	14.4	2.1	1.0	1.3	2.5	6.5	5.5
GO:0010200	response to chitin	226	0.0	10.6	0.6	0.0	0.0	0.0	0.3	0.2
GO:0009751	response to salicylic acid stimulus	304	0.2	10.5	0.3	0.1	0.2	0.0	0.0	0.1
GO:0010035	response to inorganic substance	975	3.6	4.6	1.1	0.8	2.0	2.7	10.4	10.2
GO:0010038	response to metal ion	793	2.9	5.7	2.0	0.8	2.6	2.2	4.4	7.8
GO:0046686	response to cadmium ion	622	2.6	6.2	2.3	1.3	1.9	1.7	4.3	8.9
GO:0009607	response to biotic stimulus	1470	3.0	20.3	2.4	0.3	0.0	0.1	1.1	0.0
GO:0051707	response to other organism	1417	3.3	19.3	2.8	0.2	0.0	0.1	1.0	0.0
GO:0009617	response to bacterium	582	3.7	13.4	2.2	0.1	0.3	1.1	0.5	1.2
GO:0009620	response to fungus	491	1.8	17.0	1.6	0.3	0.0	0.0	0.0	0.0
GO:0009628	response to abiotic stimulus	2953	5.4	0.2	2.3	0.6	3.1	3.9	15.3	1.7
GO:0009266	response to temperature stimulus	848	3.2	0.0	1.0	0.2	0.1	2.2	27.9	1.8
GO:0009642	response to light intensity	163	0.4	0.4	0.0	0.0	0.0	2.0	13.3	0.0
GO:0009644	response to high light intensity	93	0.7	0.7	0.0	0.0	0.0	1.9	10.8	0.1
GO:0033036	macromolecule localization	964	1.6	0.5	4.0	0.0	2.7	0.8	0.3	1.3
GO:0008104	protein localization	685	1.4	0.2	2.4	0.0	3.8	0.5	0.3	2.3
GO:0045184	establishment of protein localization	649	1.7	0.1	2.8	0.0	4.2	0.6	0.3	1.9
GO:0015031	protein transport	649	1.7	0.1	2.8	0.0	4.2	0.6	0.3	1.9
GO:0051234	establishment of localization	3119	1.5	1.8	5.9	0.0	1.8	1.3	0.5	2.7
GO:0006810	transport	3102	1.4	1.7	5.8	0.0	1.9	1.2	0.5	2.8
GO:0042044	fluid transport	54	0.7	0.1	1.6	4.0	0.0	0.0	1.1	0.2
GO:0006833	water transport	54	0.7	0.1	1.6	4.0	0.0	0.0	1.1	0.2
GO:0043900	regulation of multi-organism process	57	0.1	10.4	0.0	0.0	0.0	0.0	0.0	0.2
GO:0050790	regulation of catalytic activity	318	0.8	0.2	0.0	4.0	1.3	0.5	0.0	0.1
GO:0043086	negative regulation of catalytic activity	142	0.3	0.0	0.0	7.3	0.6	1.2	0.3	0.0
GO:0051246	regulation of protein metabolic process	285	0.0	0.3	0.6	0.0	5.3	1.2	0.8	1.0
GO:0065009	regulation of molecular function	357	1.3	0.1	0.0	4.1	1.2	0.3	0.0	0.1
GO:0044092	negative regulation of molecular function	156	0.7	0.0	0.0	6.9	0.5	1.1	0.2	0.0
GO:0016043	cellular component organization	2051	5.6	0.2	0.9	0.3	2.3	2.1	0.1	1.9
GO:0045229	external encapsulating structure organization	176	1.3	0.0	1.3	4.6	0.3	0.0	0.2	0.0
GO:0071555	cell wall organization	282	1.2	0.6	1.9	5.1	0.1	0.0	0.1	0.0

GO	Term	No. in genome	Royal blue (I)	Green (II)	Blue (V)	Cyan (VI)	Brown (VII)	Red (IX)	Yellow (XII)	Pink (XIII)
GO:0006807	nitrogen compound metabolic process	5963	1.6	0.0	0.1	0.0	3.6	0.0	1.2	8.7
GO:0034641	cellular nitrogen compound metabolic process	5863	1.4	0.0	0.1	0.0	3.6	0.0	1.3	9.2
GO:0006139	nucleobase-containing compound metabolic proc	5031	0.4	0.0	0.0	0.0	3.9	0.0	0.7	4.0
GO:0009116	nucleoside metabolic process	112	1.1	0.3	0.0	0.6	0.3	0.3	5.9	1.9
GO:0044271	cellular nitrogen compound biosynthetic process	862	1.8	0.8	1.3	0.0	0.2	3.1	2.8	7.3
GO:0009308	amine metabolic process	782	3.3	0.0	2.5	0.1	0.6	0.2	1.4	6.5
GO:0044106	cellular amine metabolic process	701	2.4	0.0	2.8	0.1	0.6	0.3	1.6	7.6
GO:0006520	cellular amino acid metabolic process	652	2.5	0.0	2.8	0.0	0.8	0.3	1.7	7.3
GO:0009309	amine biosynthetic process	357	1.3	0.0	0.7	0.4	0.4	0.3	1.1	5.6
GO:0008652	cellular amino acid biosynthetic process	331	1.3	0.0	0.7	0.2	0.5	0.4	1.3	5.5
GO:0044237	cellular metabolic process	13214	6.5	5.6	3.8	0.1	2.9	2.4	1.0	10.0
GO:0015979	photosynthesis	284	1.2	0.1	0.0	0.0	0.0	19.6	0.3	2.5
GO:0042180	cellular ketone metabolic process	1424	2.0	0.2	6.2	2.2	0.5	0.9	0.7	3.4
GO:0044255	cellular lipid metabolic process	1034	0.8	0.9	1.6	4.9	0.2	0.6	0.2	0.2
GO:0044262	cellular carbohydrate metabolic process	927	8.5	1.5	4.8	3.7	0.0	0.9	0.4	1.9
GO:0005996	monosaccharide metabolic process	287	3.2	0.4	4.1	1.9	0.0	2.5	1.0	4.0
GO:0019318	hexose metabolic process	221	1.5	0.6	2.5	1.3	0.1	2.8	1.2	4.7
GO:0006006	glucose metabolic process	150	1.1	0.0	2.2	2.0	0.3	1.6	0.8	5.9
GO:0019321	pentose metabolic process	62	1.9	0.3	4.0	1.0	0.0	0.0	0.9	3.2
GO:0046483	heterocycle metabolic process	1106	2.0	0.4	2.1	0.0	0.6	1.5	3.3	6.3
GO:0051186	cofactor metabolic process	436	0.8	0.0	2.4	0.2	1.7	0.3	4.6	5.4
GO:0006732	coenzyme metabolic process	266	1.1	0.0	3.7	0.4	1.9	0.0	3.8	7.0
GO:0006082	organic acid metabolic process	1388	2.1	0.2	5.7	2.3	0.4	1.0	0.8	3.3
GO:0043436	oxoacid metabolic process	1387	2.1	0.2	5.7	2.3	0.4	1.0	0.8	3.3
GO:0019752	carboxylic acid metabolic process	1387	2.1	0.2	5.7	2.3	0.4	1.0	0.8	3.3
GO:0032787	monocarboxylic acid metabolic process	730	0.3	1.4	2.8	4.1	0.0	1.2	0.1	0.1
GO:0006091	generation of precursor metabolites and energy	425	0.4	0.0	0.8	0.8	0.9	15.1	0.0	2.7
GO:0019684	photosynthesis, light reaction	174	1.3	0.1	0.0	0.0	0.0	16.1	0.0	1.6
GO:0009767	photosynthetic electron transport chain	76	1.0	0.2	0.0	0.0	0.4	10.2	0.1	0.1
GO:0022900	electron transport chain	122	0.6	0.1	0.0	0.0	1.5	10.6	0.1	0.2
GO:0006725	cellular aromatic compound metabolic process	776	0.4	3.5	4.6	0.6	0.2	0.2	0.5	1.2
GO:0006793	phosphorus metabolic process	2699	0.4	27.4	1.0	0.7	0.0	0.0	0.0	0.0
GO:0006796	phosphate metabolic process	2697	0.4	27.5	0.9	0.7	0.0	0.0	0.0	0.0
GO:0016310	phosphorylation	2541	0.1	27.3	0.8	1.0	0.0	0.0	0.0	0.0
GO:0044238	primary metabolic process	13429	7.7	3.8	3.4	2.8	1.4	0.6	0.9	7.1
GO:0005975	carbohydrate metabolic process	1529	12.2	2.4	5.0	7.3	0.0	0.5	1.1	0.7
GO:0006629	lipid metabolic process	1512	0.4	1.3	1.7	9.5	0.1	0.2	0.0	0.3
GO:0044281	small molecule metabolic process	6855	1.8	0.0	1.0	0.2	4.6	0.2	1.1	7.2
GO:0006066	alcohol metabolic process	483	2.7	1.0	3.7	2.9	0.1	1.0	0.5	3.8
GO:0055114	oxidation-reduction process	2206	1.7	2.7	3.1	3.1	0.9	7.2	1.5	1.4
GO:0009056	catabolic process	1618	9.4	0.4	2.2	0.8	2.8	1.3	1.2	3.6
GO:0009057	macromolecule catabolic process	578	6.5	0.0	0.5	0.0	5.4	0.2	0.5	1.2
GO:0000272	polysaccharide catabolic process	68	5.6	3.0	0.8	0.0	0.0	0.0	0.8	0.0

GO	Term	No. in genome	Royal blue (I)	Green (II)	Blue (V)	Cyan (VI)	Brown (VII)	Red (IX)	Yellow (XII)	Pink (XIII)
GO:0030163	protein catabolic process	447	4.2	0.0	0.5	0.0	6.2	0.5	0.5	1.8
GO:0044257	cellular protein catabolic process	395	3.2	0.0	0.6	0.0	6.0	0.4	0.7	1.8
GO:0051603	proteolysis involved in cellular protein catabolic p	385	2.4	0.0	0.7	0.0	6.3	0.3	0.7	1.9
GO:0044265	cellular macromolecule catabolic process	451	2.6	0.0	0.4	0.0	6.2	0.3	0.4	1.7
GO:0043632	modification-dependent macromolecule catabolic	374	2.6	0.0	0.7	0.0	6.5	0.3	0.8	1.6
GO:0044248	cellular catabolic process	1206	4.6	0.4	1.2	0.4	4.2	0.4	1.5	2.2
GO:0009058	biosynthetic process	7157	2.3	0.0	3.1	0.3	0.8	0.9	0.5	6.6
GO:0006633	fatty acid biosynthetic process	324	0.6	1.7	2.6	3.9	0.0	0.1	0.2	0.0
GO:0016109	tetraterpenoid biosynthetic process	50	0.8	0.1	0.7	0.0	0.3	3.1	0.2	0.2
GO:0000271	polysaccharide biosynthetic process	224	5.9	0.2	1.1	2.4	0.0	0.0	0.0	0.5
GO:0033692	cellular polysaccharide biosynthetic process	220	6.0	0.2	1.1	2.5	0.0	0.0	0.0	0.5
GO:0009250	glucan biosynthetic process	140	6.1	0.2	0.3	1.4	0.0	0.2	0.1	1.1
GO:0006412	translation	814	0.4	0.0	0.8	0.0	1.9	2.7	0.0	2.6
GO:0006413	translational initiation	101	1.3	0.0	0.4	0.0	2.0	3.2	0.9	0.0
GO:0016051	carbohydrate biosynthetic process	464	7.7	0.5	3.3	2.6	0.0	0.1	0.3	1.3
GO:0034637	cellular carbohydrate biosynthetic process	381	7.0	0.4	3.6	2.7	0.0	0.0	0.1	0.5
GO:0044249	cellular biosynthetic process	6940	1.7	0.0	2.8	0.3	0.8	0.9	0.4	5.7
GO:0019438	aromatic compound biosynthetic process	545	0.8	3.7	6.1	1.0	0.0	0.2	0.2	1.1
GO:0009699	phenylpropanoid biosynthetic process	362	0.4	1.9	5.2	1.4	0.0	0.5	0.4	0.1
GO:0009813	flavonoid biosynthetic process	186	0.2	1.1	6.6	0.3	0.0	0.1	0.1	0.2
GO:0051188	cofactor biosynthetic process	287	0.2	0.3	1.8	0.3	1.3	0.9	5.1	2.5
GO:0009108	coenzyme biosynthetic process	158	0.3	0.0	2.5	0.8	1.0	0.0	3.7	2.9
GO:0009698	phenylpropanoid metabolic process	458	0.2	1.6	4.1	1.3	0.1	0.4	0.6	0.2
GO:0009812	flavonoid metabolic process	215	0.1	1.2	6.7	0.2	0.1	0.0	0.4	0.1
GO:0005976	polysaccharide metabolic process	367	9.0	1.0	1.2	2.8	0.0	0.1	0.6	0.1
GO:0044042	glucan metabolic process	243	7.9	0.1	0.5	2.2	0.0	0.3	0.5	0.4
GO:0006073	cellular glucan metabolic process	233	7.7	0.2	0.3	2.3	0.0	0.3	0.5	0.4
GO:0005982	starch metabolic process	75	9.2	0.0	0.7	0.3	0.0	0.0	0.7	0.0
GO:0044264	cellular polysaccharide metabolic process	314	6.8	0.2	1.0	3.3	0.0	0.1	0.2	0.2
GO:0006464	protein modification process	3771	0.1	21.1	1.7	0.4	0.0	0.2	0.0	0.1
GO:0018193	peptidyl-amino acid modification	157	0.3	0.5	0.1	0.1	0.0	6.3	0.1	1.8
GO:0006468	protein phosphorylation	2397	0.0	28.5	1.0	1.0	0.0	0.0	0.0	0.0
GO:0043687	post-translational protein modification	69	0.1	0.3	1.7	0.0	3.7	0.5	3.5	0.1
GO:0044267	cellular protein metabolic process	5221	1.5	12.0	1.7	0.0	0.7	1.5	0.0	2.1
GO:0006457	protein folding	388	3.6	0.3	0.0	0.0	0.3	1.9	12.3	3.6
GO:0043412	macromolecule modification	3978	0.1	19.4	1.4	0.3	0.0	0.1	0.0	0.1
GO:0007154	cell communication	2782	0.0	16.6	1.0	0.4	0.2	0.0	0.0	0.0
GO:0007165	signal transduction	2295	0.0	12.5	0.4	0.7	0.3	0.0	0.0	0.0
GO:0016049	cell growth	507	1.6	2.1	0.1	3.3	1.5	0.5	0.0	1.6
GO:0048767	root hair elongation	69	1.7	0.0	0.0	3.5	0.4	0.2	0.4	0.5
GO:0045454	cell redox homeostasis	183	1.8	4.6	0.7	0.1	1.0	2.8	1.6	1.0
GO:0051641	cellular localization	874	2.3	0.2	1.6	0.0	4.5	1.5	0.5	2.5
GO:0051649	establishment of localization in cell	789	2.1	0.2	1.2	0.0	5.3	1.7	0.8	2.5

GO	Term	No. in genome	Royal blue (I)	Green (II)	Blue (V)	Cyan (VI)	Brown (VII)	Red (IX)	Yellow (XII)	Pink (XIII)
GO:0046907	intracellular transport	690	1.0	0.1	1.1	0.0	6.1	1.9	1.0	3.3
GO:0006886	intracellular protein transport	481	0.6	0.2	1.6	0.0	5.1	0.1	0.1	1.5
GO:0070727	cellular macromolecule localization	551	0.8	0.2	2.2	0.0	4.3	0.1	0.0	1.7
GO:0034613	cellular protein localization	511	0.5	0.2	1.4	0.0	4.6	0.1	0.1	1.9
GO:0051716	cellular response to stimulus	3247	0.7	12.7	0.1	0.4	1.2	0.0	0.0	0.0
GO:0034599	cellular response to oxidative stress	52	2.3	0.1	0.3	0.0	0.7	3.0	0.2	0.6
GO:0071841	cellular component organization or biogenesis	1990	5.0	0.0	0.8	0.0	1.1	3.0	0.0	2.1
GO:0007047	cellular cell wall organization	132	2.1	0.0	1.7	4.7	0.7	0.0	0.3	0.0
GO:0009664	plant-type cell wall organization	114	1.0	0.0	1.6	3.3	0.6	0.0	0.4	0.0
GO:0009657	plastid organization	263	5.6	0.2	0.9	0.0	0.1	5.1	0.0	0.8
GO:0009658	chloroplast organization	184	2.9	0.0	0.7	0.0	0.2	4.8	0.1	0.4

The 20-most over-represented Biological Process GO terms from eight network modules were extracted and combined. Only GO terms from hierarchy levels 3-7, and with at least 50 genes were included. The negative log10 transformed *p* values derived from significance test of GO enrichment are shown by heatmap.

Supplemental Table 3. List of NRX1 probes, their gene model matches and sequence identity matrix.[a]

Probe	Sequence	Best Gene Model(s)	Name	NRX1.1	NRX1.2	NRX1.3	NRX1.4	NRX1.5	NRX1.6	NRX1.7	NRX1.8	NRX1.9	NRX1.10
pt2_24428	ATGGCTGTCGTGGAACAGGACATAGTTGGTCTT TCTATTGCAAACAATGTGACTTTGATC	POPTR_0010s06930; POPTR_0010s06940	NRX1.1/1.2[b]	**100**	**100**					98		93	
pt2_24429	ATTTACACCGGAAAAGCTTGACGAGCTCGCTGA CATTAAAAGGGCAAAACTGGAATCGCA	POPTR_0010s06950	NRX1.3	93	93	**100**	88		88	88	88		
pt2_24430	AAACACGAACTTCATACTGAGCATGAGCTGATA CGTACTAAACGCAGTGCATACGGTTGC	POPTR_0010s06960	NRX1.4	77	77	77	**100**		98	75	77	77	
pt2_24431	AATGGGGAAAATGATTTTGTGATTGGCAAAAGT GGCTCCAAGGTCCCAGTGTCCGATCTA	POPTR_0010s06950; POPTR_0010s06970	NRX1.3/1.5	93	93	**100**	87	**100**	97		87	87	
pt2_24432	AAACACGAACTACATACTGAGCATGAGCTGATA CGTACTAAACGCAGTGCATACGGTTGC	POPTR_0010s06980	NRX1.6	75	75	75	98		**100**	73	75	75	
pt2_24433	TAGAAAAGGCAAAACTGGAATCGCAGACGCTTG AATCAGTTTTGGTTATTGGGGAGGCTC	POPTR_0010s06990	NRX1.7	87	87	83	87	87	87	**100**	87	87	
pt2_24434	CTGTGGGGAAACTGGAAATAGGTGGTCTTTCTA TTGCAAACAATGTGACTTTGATCTTCA	POPTR_0010s07000	NRX1.8	70	70	98	97		95	70	**100**	70	
pt2_24435	AAGCAAAAGACAATGCAGTTGAGGTGATCTTCA TCTCAAGTGACAGCGATCAAACCACCT	POPTR_0010s07010	NRX1.9[c]	97	97	98	85	87	85	90	87	**100**	
pt2_21490	CCAGAGAAAGTGAAACACGAACTTCATGCTGAA CATGAGCTTATACGTTCTAAACACTAA	POPTR_0008s17570	NRX1.10[c]	85	85	85	85		83		85	85	**100**

[a] Sequence identity less than 70% is not shown.

[b] NRX1.2 (POPTR_0010s06940) is nearly identical to NRX1.1.

[c] NRX1.9 and NRX1.10 represent partial/truncated sequences

Supplemental Table 4. List of microarray comparisons used in the meta-analysis.

No.[a]	GEO accession	Stress	n[b]	Control sample description with a representative GEO accession no.	Stressed sample description with a representative GEO accession no.	No. overlap		% overlap	
						driver[c]	hub[d]	driver[c]	hub[d]
1	GSE42511	SA	2	GSM1041235_WT_NT	GSM1041219_F52_NT	41	256	28%	58%
2	GSE42511	SA+heat	2	GSM1041233_WT_HT	GSM1041217_F52_HT	88	373	61%	85%
3	GSE42511	SA	2	GSM1041235_WT_NT	GSM1041223_F10_NT	102	366	71%	84%
4	GSE42511	SA+heat	2	GSM1041233_WT_HT	GSM1041221_F10_HT	130	422	90%	96%
5	GSE42511	heat	2	GSM1041235_WT_NT	GSM1041233_WT_HT	32	237	22%	54%
6	GSE15242	drought	3	GSM377359_DN34_midnight_well.watered	GSM377362_DN34_midnight_water.limited	55	220	38%	50%
7	GSE15242	drought	3	GSM377365_DN34_predawn_well.watered	GSM377378_DN34_predawn_water.limited	45	179	31%	41%
8	GSE15242	drought	3	GSM377381_DN34_midday_well.watered	GSM377384_DN34_midday_water.limited	62	247	43%	56%
9	GSE15242	drought	3	GSM377390_DN34_lateday_well.watered	GSM377393_DN34_lateday_water.limited	61	234	42%	53%
10	GSE15242	drought	3	GSM377396_NM6_midnight_well.watered	GSM377408_NM6_midnight_water.limited	66	240	46%	55%
11	GSE15242	drought	3	GSM377412_NM6_predawn_well.watered	GSM378177_NM6_predawn_water.limited	39	155	27%	35%
12	GSE15242	drought	3	GSM378180_NM6_midday_well.watered	GSM378183_NM6_midday_water.limited	55	248	38%	57%
13	GSE15242	drought	3	GSM378186_NM6_lateday_well.watered	GSM378189_NM6_lateday_water.limited	57	225	40%	51%
14	GSE16783	wound[e]	2	GSM421464_Clone.RM5_LPI5_C_1wk	GSM421466_Clone.RM5_LPI5_W_1wk	62	252	43%	58%
15	GSE16783	wound[e]	2	GSM421468_Clone.RM5_LPI1_C_1wk	GSM421470_Clone.RM5_LPI1_W_1wk	25	155	17%	35%
16	GSE16785	wound[e]	2	GSM421477_Clone.RM5_LPI5_C_90h	GSM421479_Clone.RM5_LPI5_W_90h	45	190	31%	43%
17	GSE17226	drought	2	GSM431450_CCTL08L	GSM431448_CWD08L	57	215	40%	49%
18	GSE17226	drought	2	GSM431453_SCTL08L	GSM431455_SWD08L	54	222	38%	51%
19	GSE17230	drought	2	GSM431485_CCTLL	GSM431488_CAMIL	60	217	42%	50%
20	GSE17230	drought	2	GSM431485_CCTLL	GSM431484_CAMOL	59	217	41%	50%
21	GSE17230	drought	2	GSM431485_CCTLL	GSM431487_CEARL	63	223	44%	51%
22	GSE17230	drought	2	GSM431479_SCTLL	GSM431480_SAMIL	57	217	40%	50%
23	GSE17230	drought	2	GSM431479_SCTLL	GSM431489_SAMOL	57	219	40%	50%
24	GSE17230	drought	2	GSM431479_SCTLL	GSM431490_SEARL	60	221	42%	50%
25	GSE21171	drought	3	GSM529887_AP.947_well.watered_predawn	GSM529890_AP.947_water.limited_predawn	38	203	26%	46%
26	GSE21171	drought	3	GSM529941_AP.2298_well.watered_midday	GSM529944_AP.2298_water.limited_midday	44	221	31%	50%
27	GSE21171	drought	3	GSM529947_AP.2300_well.watered_predawn	GSM529950_AP.2300_water.limited_predawn	43	215	30%	49%
28	GSE21171	drought	3	GSM529953_AP.2300_well.watered_midday	GSM529956_AP.2300_water.limited_midday	41	199	28%	45%
29	GSE21171	drought	3	GSM529893_AP.947_well.watered_midday	GSM529896_AP.947_water.limited_midday	58	251	40%	57%
30	GSE21171	drought	3	GSM529899_AP.1005_well.watered_predawn	GSM529902_AP.1005_water.limited_predawn	50	240	35%	55%
31	GSE21171	drought	3	GSM529905_AP.1005_well.watered_midday	GSM529908_AP.1005_water.limited_midday	56	238	39%	54%
32	GSE21171	drought	3	GSM529911_AP.1006_well.watered_predawn	GSM529914_AP.1006_water.limited_predawn	59	248	41%	57%
33	GSE21171	drought	3	GSM529917_AP.1006_well.watered_midday	GSM529920_AP.1006_water.limited_midday	51	223	35%	51%
34	GSE21171	drought	3	GSM529923_AP.2278_well.watered_predawn	GSM529926_AP.2278_water.limited_predawn	57	245	40%	56%
35	GSE21171	drought	3	GSM529929_AP.2278_well.watered_midday	GSM529932_AP.2278_water.limited_midday	58	240	40%	55%
36	GSE21171	drought	3	GSM529935_AP.2298_well.watered_predawn	GSM529938_AP.2298_water.limited_predawn	34	184	24%	42%
37	GSE27693	drought	3	GSM685820_DN.MB.2007.am.well.watered	GSM685823_DN.MB.2007.am.water.limited	52	236	36%	54%
38	GSE27693	drought	3	GSM685874_WP.AB.2007.pm.well.watered	GSM685877_WP.AB.2007.pm.water.limited	41	195	28%	45%
39	GSE27693	drought	3	GSM685880_WP.SK.2007.am.well.watered	GSM685883_WP.SK.2007.am.water.limited	35	193	24%	44%
40	GSE27693	drought	3	GSM685886_WP.SK.2007.pm.well.watered	GSM685889_WP.SK.2007.pm.water.limited	39	198	27%	45%
41	GSE27693	drought	3	GSM685826_DN.MB.2007.pm.well.watered	GSM685829_DN.MB.2007.pm.water.limited	59	246	41%	56%
42	GSE27693	drought	3	GSM685832_DN.SK.2007.am.well.watered	GSM685835_DN.SK.2007.am.water.limited	52	226	36%	52%
43	GSE27693	drought	3	GSM685838_DN.SK.2007.pm.well.watered	GSM685841_DN.SK.2007.pm.water.limited	53	210	37%	48%
44	GSE27693	drought	3	GSM685844_WK.AB.2007.am.well.watered	GSM685847_WK.AB.2007.am.water.limited	59	230	41%	53%
45	GSE27693	drought	3	GSM685850_WK.AB.2007.pm.well.watered	GSM685853_WK.AB.2007.pm.water.limited	43	184	30%	42%
46	GSE27693	drought	3	GSM685856_WK.SK.2007.am.well.watered	GSM685859_WK.SK.2007.am.water.limited	39	203	27%	46%
47	GSE27693	drought	3	GSM685862_WK.SK.2007.pm.well.watered	GSM685865_WK.SK.2007.pm.water.limited	52	211	36%	48%
48	GSE27693	drought	3	GSM685868_WP.AB.2007.am.well.watered	GSM685871_WP.AB.2007.am.water.limited	42	212	29%	48%
49	GSE37608	drought	2	GSM923163_Control	GSM923161_Short.term.water.deficit	60	233	42%	53%
50	GSE9673	pathogen[f]	3	GSM244430_non.infected.tissue	GSM244433_Mlp.infected.tissue	66	257	46%	59%
51	GSE9673	pathogen[f]	3	GSM244430_non.infected.tissue	GSM244436_Mmd.infected.tissue	66	258	46%	59%
52	GSE9673	pathogen[f]	3	GSM244430_non.infected.tissue	GSM244439_Mixed.infected.tissue	68	262	47%	60%
53	GSE10873	ozone	3	GSM275585_Cy3_control	GSM275585_Cy5_ozone	27	95	19%	22%

[a] Comparison no. as shown in Figure 9 and Supplemental Figure 9. [b] Number of biological replicates in each group. [c-d] Number and percentage of [c] the 144 driver genes or [d] the 438 hub genes found in each comparison. [e] In the wounding experiments, a stronger response was observed in systemic LPI-5 than the more distal LPI-1 one-week after leaf wounding, and in LPI-5 one-week than 90-hour after wounding. [f] Responses of the driver/hub genes to leaf fungal pathogen were in accordance to the overall transcriptome responses, stronger in leaves infected by mixed *Melampsora* strains than by individual strains alone (Azaiez et al., 2009).

Supplemental Table 5. Primers used in this study.

Gene	Gene model or accession no.	Forward primer (5' to 3')	Reverse primer (5' to 3')	Purpose
Irp9	CAB46570	GTCGACATGAAAATCAGTGAATTTC *or* AGATCTATGAAAATCAGTGAATTTC	GCTAGCCTACACCATTAAATAGGGC	cloning
		ATGCGTTTACCGTGCTGTTTCCGT	AGGGCGCAATGCTCGCTAATTTCT	qRT-PCR
ferrodoxin (FD)	At1g60950	AGATCTAAAATGGCTTCCACTGCTCTC	GTCGACGACCTTGTATGTAGCCATGGC	cloning
NahG	M60055	AACCTCGCCGAGCTGCTTGA	AGGTCAGTGTCGAGGTCGTGGT	qRT-PCR
NRX1	POPTR_0008s17570, POPTR_0010s06930 - POPTR_0010s07010	TGCCTTGGTTAGCCCTTCCATTTG	TGTCARGTGCWTCCGAGCTTCCTT	qRT-PCR
WRKY	POPTR_0006s27950	ACCATGCTAGCCATTCTCAACCTG	TTAGCACTGTCAACGTGCATTCCA	qRT-PCR
WRKY	POPTR_0016s14490	GTGATCACGCTTCRAACAAGCCAA	TACCATCCATGTCCARACTGTGTGAG	qRT-PCR
RLK	POPTR_0012s01760	ACGCGCAAAYSGCAAAGAAGCTGA	TCTGTTTCARWGATCACYTCCAACGC	qRT-PCR
RLK	POPTR_0017s09520	TGGAGGAAGGAAGAACGTCGATGA	TGCRCTTGTTYTCTTAGGGACAGAGG	qRT-PCR
EF1-β	POPTR_0001s23190	GACCTKGTATCAGTGGATTCCCTC	GAACAGAGGCACAAGATTACCAGG	qRT-PCR
ARP	POPTR_0017s08430	ACTGTGAGGAGATGCAGAAACGCA	GCTGTGTCACGGGCATTCAATGYT	qRT-PCR
TAF	POPTR_0001s37010	CGTGCAGCTGGTCTCTRTATGTAT	ACTGACACACTGGAAGCTCCAACA	qRT-PCR

Restriction sites are underlined.